Titin visualization in real time reveals an unexpected level of mobility within and between sarcomeres

a Silva Lopes, K. and Pietas, A. and Radke, M.H. and Gotthardt, M.

This is a copy of the final article, which was first published online on 09 May 2011 and in final edited form in:

Journal of Cell Biology
2011 MAY 16 ; 193(4): 785-798
doi: 10.1083/jcb.201010099

Publisher: Rockefeller University Press

Published May 9, 2011

Titin visualization in real time reveals an unexpected level of mobility within and between sarcomeres

Katharina da Silva Lopes,[1] Agnieszka Pietas,[1] Michael H. Radke,[1] and Michael Gotthardt[1,2]

[1]Neuromuscular and Cardiovascular Cell Biology, Max-Delbrück-Center for Molecular Medicine (MDC), D-13122 Berlin-Buch, Germany
[2]Department of Veterinary and Comparative Anatomy, Pharmacology, and Physiology, Washington State University, Pullman, WA 99164

The giant muscle protein titin is an essential structural component of the sarcomere. It forms a continuous periodic backbone along the myofiber that provides resistance to mechanical strain. Thus, the titin filament has been regarded as a blueprint for sarcomere assembly and a prerequisite for stability. Here, a novel titin-eGFP knockin mouse provided evidence that sarcomeric titin is more dynamic than previously suggested. To study the mobility of titin in embryonic and neonatal cardiomyocytes, we used fluorescence recovery after photobleaching and investigated the contribution of protein synthesis, contractility, and calcium load to titin motility. Overall, the kinetics of lateral and longitudinal movement of titin-eGFP were similar. Whereas protein synthesis and developmental stage did not alter titin dynamics, there was a strong, inhibitory effect of calcium on titin mobility. Our results suggest a model in which the largely unrestricted movement of titin within and between sarcomeres primarily depends on calcium, suggesting that fortification of the titin filament system is activity dependent.

Introduction

The sarcomeric protein titin alias connectin is, after actin and myosin, the third most abundant protein in vertebrate striated muscle and expressed from mid-gestation through adult life (Fürst et al., 1989; Schaart et al., 1989). Its functional domains are assembled into various titin isoforms to adjust its mechanical and structural properties depending on developmental stage, functional requirements, and underlying disease (Neagoe et al., 2002; Lahmers et al., 2004; Opitz et al., 2004; Warren et al., 2004). The large cardiac titin N2BA isoform (3.5–3.7 MDa) is rapidly replaced by the smaller N2B isoform (3.0 MDa) both after birth and with reexpression of the fetal gene program in cardiac pathology (Neagoe et al., 2002; Lahmers et al., 2004; Makarenko et al., 2004; Opitz et al., 2004; Warren et al., 2004). This change in titin isoform expression helps adapt the elastic properties of the myocardium to enable efficient filling of the cardiac ventricle in diastole and has been characterized in detail both on the molecular and functional level (Lahmers et al., 2004; Opitz et al., 2004). Nevertheless, there is a gap in knowledge on how the altered titin isoform makeup is translated into altered sarcomeric protein composition, i.e., how titin molecules are replaced and relocalized in the working sarcomere to adapt cardiac function.

Although the maintenance and remodeling of preexisting sarcomeres and the balance of assembly and disassembly in the working myocardium are still only poorly understood, there has been considerable progress toward elucidating de novo sarcomere assembly during embryonic development (Dabiri et al., 1997; Du et al., 2003; Wang et al., 2005a,b; Weinert et al., 2006; Stout et al., 2008; Sanger et al., 2009). According to the premyofibril model, the initial formation of regular sarcomeres involves the polymerization of actin, incorporation of myosin, as well as assembly and alignment of Z-bodies, which incorporate titin's N terminus and form the future Z-disc (Rhee et al., 1994; Sanger et al., 2000; Du et al., 2003). Subsequently titin's C terminus is integrated into the M-band and connected to the muscle myosin filament (Nave et al., 1989; Obermann et al., 1996). The resulting continuous filament system has been regarded as a molecular ruler and as a blueprint for sarcomere assembly because titin's PEVK-region, immunoglobulin, fibronectin, and kinase domains are associated with specific sections of the half-sarcomere and thus sublocalize the various titin-binding proteins along the myofilament (Labeit and Kolmerer, 1995; Trinick, 1996; van der Loop et al., 1996; Obermann et al., 1997; Gregorio et al., 1998). Within the

Correspondence to Michael Gotthardt: gotthardt@mdc-berlin.de

Abbreviations used in this paper: BDM, 2,3-butanedione monoxime; CX, cycloheximide; Flp, flippase recombination enzyme; FRT, flippase recognition target; Neo, neomycin; ROI, region of interest.

Supplemental Material can be found at:
http://jcb.rupress.org/content/suppl/2011/05/06/jcb.201010099.DC1.html

The Rockefeller University Press $30.00
J. Cell Biol. Vol. 193 No. 4 785–798
www.jcb.org/cgi/doi/10.1083/jcb.201010099

Published May 9, 2011

Z-disc, titin binds to T-cap alias telethonin (Gregorio et al., 1998), which assembles titin's N terminus into an antiparallel sandwich complex (Zou et al., 2006). Titin's structural relations to the thin filament are mediated by α-actinin, which connects to titin in the Z-disc (Ohtsuka et al., 1997a,b; Sorimachi et al., 1997). The interaction between titin's PEVK region and actin within the I-band is calcium dependent and has been related to the passive properties of the sarcomere and its relaxation kinetics (Kulke et al., 2001; Yamasaki et al., 2001). Within the A-band titin is tightly linked to the thick filament via its multiple binding sites for myosin-binding protein C (MyBP-C; Labeit et al., 1992; Houmeida et al., 1995; Freiburg and Gautel, 1996). The titin–myosin interaction is reinforced at the M-band where titin interacts with myomesin and M-protein—both relevant for the assembly and structural maintenance of thick filaments (Bähler et al., 1985; Nave et al., 1989; Vinkemeier et al., 1993; Obermann et al., 1996). Thus, titin's integration into the sarcomeric lattice is mediated by its interaction with multiple structural proteins along the half-sarcomere and provides an elastic connection between the thick and thin filament systems, thereby centering the A-band in the sarcomere (Houmeida et al., 1995).

In addition to its structural functions, titin relates to signal transduction and metabolism through its kinase domain, phosphorylation sites, and interaction with adaptor and signaling proteins. Four-and-a-half LIM domain protein 2 (FHL2) recruits metabolic enzymes to sites of high energy consumption such as the M-band and the cardiac N2B region within the I-band (Lange et al., 2002). Titin's N2A region binds muscle ankyrin repeat proteins, which link myofibrillar stretch-induced signaling pathways and muscle gene expression (Miller et al., 2003) and the protease calpain 3 (p94), which has been suggested to play a role in myofibrillogenesis and sarcomere remodeling (Sorimachi et al., 1995; Kramerova et al., 2004). Additional binding sites for proteins related to signal transduction and protein degradation, such as MuRF (muscle-specific RING finger protein) 1 and 2 and calpain 3 are located at titin's M-band (Kinbara et al., 1997; Centner et al., 2001; Lange et al., 2002; Witt et al., 2005). Thus, multiple binding proteins integrate titin into the sarcomere and decorate the titin filament with links to basic cellular functions such as trophic signaling and energy balance.

Although the mature myofibril appears as a stable structure, it is crucial that its components can readily detach, not only to replace proteins but also to adapt in conditions that require atrophy or hypertrophy. Thus, cardiac proteins are actively exchanged between organized structures such as the sarcomere and cytoplasmic pools (McKenna et al., 1985a; Sanger et al., 1986; Mittal et al., 1987). Within a few hours after injection, fluorescently labeled proteins are properly incorporated into the sarcomere (McKenna et al., 1985b; Mittal et al., 1987; Dome et al., 1988). The dynamics of proteins within the sarcomere as determined by photobleaching (exchange of bleached by neighboring fluorescent molecules) was reported to be much faster than expected based on their protein half-lives in the order of several days (Zak et al., 1977; Suzuki et al., 1998; Hasebe-Kishi and Shimada, 2000; Wang et al., 2005a; Skwarek-Maruszewska et al., 2009). Although the mobility of various titin-binding proteins has been investigated and related to sarcomere stability, stress, and signal transduction (McElhinny et al., 2002; Pizon et al., 2002; Miller et al., 2003), it has so far not been possible to obtain similar data for titin itself based on technical challenges related to titin's exceptional size.

Here, we have generated a titin-eGFP knockin mouse and used fluorescence recovery after photobleaching (FRAP) to study titin dynamics in living cells. We were able to dissect titin mobility from de novo protein synthesis and demonstrated that the migration of titin molecules depends on calcium. We show that titin moves equally efficient within and between adjacent sarcomeres and that this process does not depend on cardiomyocyte contraction or major rearrangements of the myofilament. Furthermore, we provide evidence that titin dynamics are independent from the developmental stage as embryonic and neonatal cardiomyocytes display similar titin mobility. Our data suggest that titin molecules are rapidly exchanged between a pool of sarcomeric (bound) and nonsarcomeric (free) titin and that its mobility is inversely correlated with calcium levels but maintained from embryonic to postnatal development.

Results

Generation and validation of the animal model

Due to its size of up to 3.7 MDa, titin is not readily available for overexpression, gain-of-function studies, or the generation of a tagged full-length protein. To circumvent this problem, we have used gene targeting of the titin locus and generated a fluorescently labeled titin protein for expression analysis and real-time imaging. The targeting vector (Fig. 1 A) was designed to integrate eGFP into titin's M-band exon 6 with a Neo resistance gene inserted into the 3′-untranslated region. After electroporation, selection, and verification of the targeted allele, positive embryonic stem cells were injected into blastocysts as described previously (Gotthardt et al., 2003). After germline transmission and excision of the Neo resistance cassette, subsequent generations were bred to hetero- or homozygosity as experiments warranted. Knockin, heterozygous, and wild-type animals were born at the expected Mendelian ratios. Both hetero- and homozygotes were viable and fertile, without any obvious phenotypic defects or changes in heart to body weight ratio (Fig. 1, B and C). Expression of titin-eGFP was confirmed by qPCR and Western blot, which both resulted in a strong signal in homozygote and an intermediate expression in heterozygote animals (Fig. 1, D and E; Fig. S1). The robust expression of titin-eGFP protein allowed for the detection of the native eGFP-fusion protein even in heterozygotes (Fig. 1 F). The periodic distribution of the fluorescent signal as detected by confocal imaging suggested proper integration of titin-eGFP into the sarcomere, which was confirmed by coimmunofluorescence staining (Fig. 2). The alternating signal of titin-eGFP at the M-band and the Z1/Z2 titin epitope or α-actinin at the Z-disc documented proper integration of the extended titin molecule in the Z-disc and M-band of the sarcomere and the expected localization of the eGFP-tag at the M-band in heart, quadriceps, and soleus muscle.

Published May 9, 2011

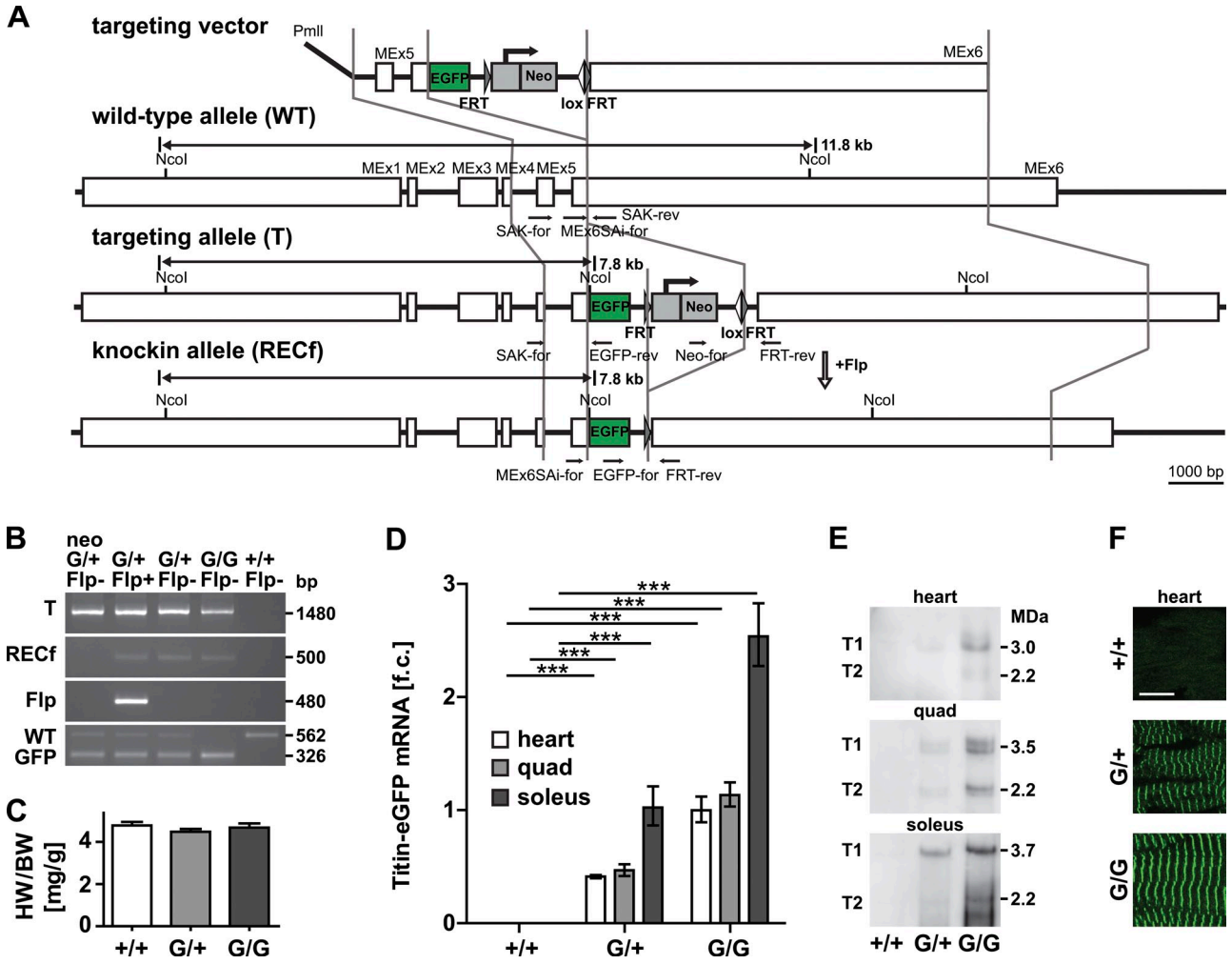

Figure 1. **Generation of the titin-eGFP knockin mouse.** (A) Targeting strategy to insert eGFP into titin's M-band exon 6 (MEx6). The targeting vector was linearized with PmlI and contains the FRT flanked Neo selectable marker. Locations of the genotyping primers are indicated in the wild-type, targeted, and knockin allele (black arrows). Germline expression of the Flp recombinase was used to excise the Neo cassette (open arrow). (B) PCR-based genotyping of wild-type (+/+), heterozygous (G/+), and homozygous (G/G) titin-eGFP knockin mice. The targeted allele (T) and the excision of the Neo cassette (RECf allele) after introduction of the Flp transgene (Flp) were confirmed by PCR. Homozygous knockin animals are viable as documented by the absence of the wild-type allele in the GFP-positive animal (G/G Flp−). Bp, base pair. (C) Heart to body weight ratio of female heterozygous (G/+) and homozygous (G/G) titin-eGFP knockin mice was unchanged compared with wild-type (+/+; $n = 6$ per group). (D) Expression analysis of titin-eGFP in heart and skeletal muscle (quadriceps and soleus) using qRT-PCR confirmed the expected intermediate titin-eGFP mRNA levels in heterozygous (G/+) versus homozygous animals (G/G). Soleus muscle mRNA levels were increased as compared with heart and quadriceps. Data were normalized to 18S RNA and titin levels in homozygous hearts were set as 1 ($n = 5$ per group). f.c., fold change. ***, $P < 0.001$. (E) Western blot using an anti-GFP antibody detects the high molecular weight titin-eGFP fusion protein (T1, full length; T2, degradation product). (F) The eGFP-tagged titin protein was integrated into the sarcomere as indicated by confocal imaging of native cardiac tissue. In both hetero- and homozygotes, the fluorescent signal was sufficiently strong for detection without amplification. Bar, 10 µm. Error bars indicate SEM.

The expression of titin-eGFP from the endogenous promoter at physiological levels, the proper assembly of the eGFP-tagged sarcomeres, and the lack of an apparent phenotype in hetero- or homozygote animals make the established animal model a suitable tool not only to follow expression and localization of titin in different muscle types (skeletal muscle and heart), but also to investigate titin dynamics in living cardiomyocytes.

Kinetics of titin-eGFP mobility in embryonic cardiomyocytes

To facilitate real-time imaging and obtain a baseline reading of titin's mobility, we used primary cultures of embryonic cardiomyocytes isolated at embryonic day 13.5 (E13.5). The continued and regular beating of cardiomyocytes after isolation and plating was used to assess the quality of the culture. We used FRAP as a parameter of titin mobility with a minimal region of interest (ROI) that comprises one sarcomere length to reduce phototoxicity. Our preliminary analysis indicated stable recovery within 14 h. Calculated half-fluorescence mobility and mobile fractions did not change with an additional incubation through 24 h. Although myocytes contract and shift position in culture over time, the area of photobleaching was stable throughout the experiment. Based on these experiments we used homozygous titin-eGFP knockin cardiomyocytes to increase the signal-to-noise ratio and followed the exchange of bleached by unbleached titin-eGFP molecules for 14 h to reach a steady state of recovery (Fig. 3 A) and reduce the possibility for changes in the cellular phenotype in culture. To distinguish changes in the eGFP signal

Published May 9, 2011

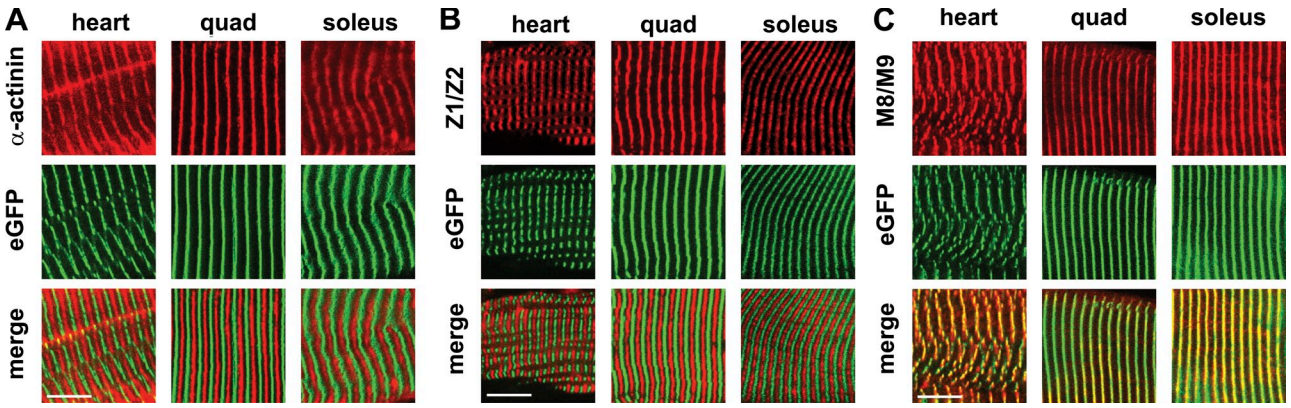

Figure 2. **Integration of titin-eGFP into the sarcomere.** Expression and localization of titin-eGFP were documented in the heart, quadriceps, and soleus of homozygous, adult knockin mice. Coimmunofluorescence staining with antibodies directed against the Z-disc protein α-actinin (A), titin's Z1/Z2 epitope (B), and titin's M-band epitope M8/M9 (C) confirmed that titin-eGFP was properly integrated into the Z-disc and M-band of the sarcomere where it colocalized with the M8/M9 epitope in all striated muscle tissues analyzed. Bar, 10 µm.

that result from protein synthesis versus protein mobility, we used cycloheximide (CX) as an inhibitor of protein synthesis that blocks translation elongation and has been applied to embryonic as well as to neonatal cardiomyocytes (Zaal et al., 1999; Wang et al., 2005a; Stahlhut et al., 2006). CX was added to the media 1 h before photobleaching and continued throughout the experiment. Fluorescence recovery rates were obtained by plotting the green fluorescence signal as a function of time after photobleaching. FRAP analysis of control cells (without treatment) as compared with CX-treated cells resulted in similar kinetics with complete fluorescence recovery after 14 h. Analysis of the recovery profile indicated no significant change in mobile fractions (49 ± 4% vs. 53 ± 9%) or half-lives of fluorescence recovery (2.2 vs. 2.6 h) in control compared with CX-treated cells (Fig. 3, B and C; Table I).

To dissect the contribution of sarcomere rearrangement versus molecular movement of titin-eGFP, we increased the ROI as indicated in Fig. 4. The mobile fraction was unchanged

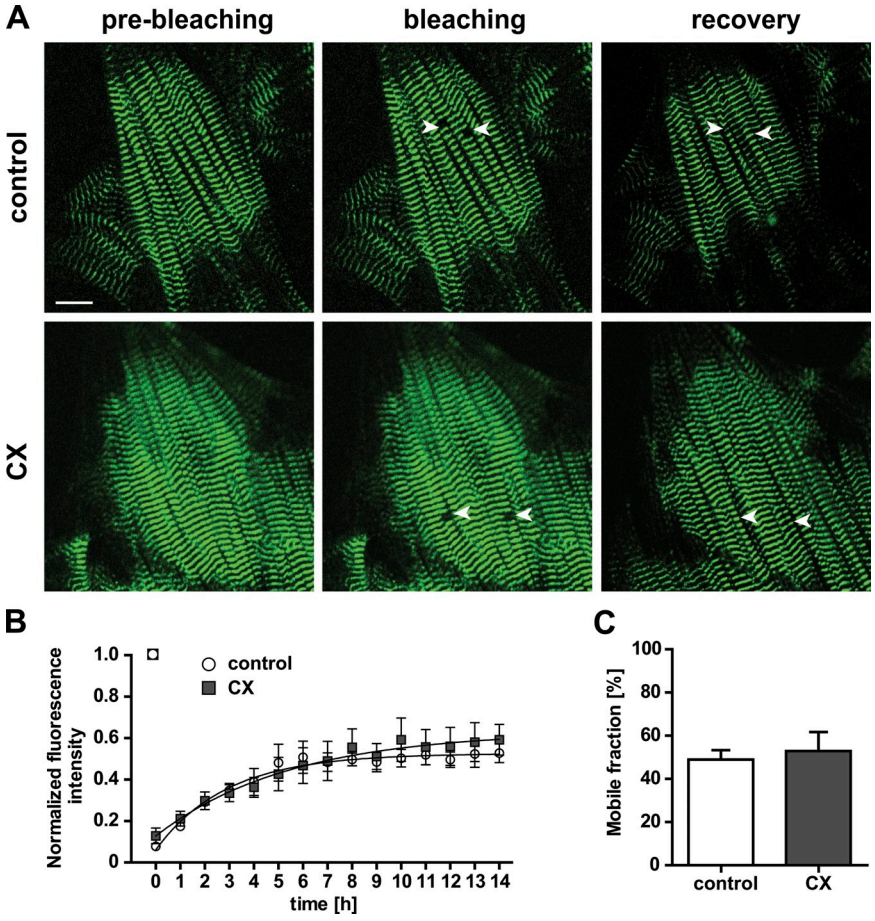

Figure 3. **Titin-eGFP dynamics are independent from protein synthesis.** Cells were imaged for 14 h after photobleaching to follow recovery and treated with cycloheximide (CX) to distinguish titin mobility and de novo synthesis. (A) Images of control and CX-treated embryonic cardiomyocytes (E13.5) from homozygous titin-eGFP knockin mice were obtained before and immediately after bleaching (white arrows). Titin-eGFP was homogenously distributed in embryonic cardiomyocytes and fluorescence had significantly recovered after 14 h. Bar, 10 µm. (B) Plot of fluorescence intensity vs. time after photobleaching to compare titin-eGFP protein recovery of control and CX-treated cells. Inhibition of protein synthesis did not influence the mobility of titin-eGFP (control, $n = 4$; CX, $n = 3$). (C) Quantification of the titin-eGFP mobile fractions indicated a level of ~50% in both control and CX-treated cardiomyocytes (control, $n = 4$; CX, $n = 3$). Error bars indicate SEM.

Published May 9, 2011

Table I. **Mobile fractions (M_f) and exchange half-lives ($t_{1/2}$) of titin-eGFP (FRAP analysis)**

Treatment or cell type	M_f [%]	$t_{1/2}$ [h]
Control	49 ± 4	2.1 ± 0.4
CX	53 ± 9	2.6 ± 0.4
LCa	72 ± 4**	3.6 ± 0.6
HCa	28 ± 5*	2.9 ± 0.9
BDM	38 ± 1	2.3 ± 0.3
BDM + HCa	24 ± 1*	1.7 ± 0.8
NCM	56 ± 3	3.7 ± 0.4

Control, embryonic cardiomyocytes without treatment at normal calcium (NCa); CX, cycloheximide treatment; LCa, low calcium concentration; HCa, high calcium concentration; BDM, 2,3-butanedione monoxime; NCM, neonatal cardiomyocytes (n = 24).

*, $P < 0.05$.

**, $P < 0.01$; one-way ANOVA, posttest Dunnett (comparison vs. control). Data are indicated as means ± SEM.

between small, medium, and large bleached areas, suggesting that the relative amount of titin-eGFP that can move into the bleached ROI is independent from the size of the area. The calculated exchange half-life is increased with the area of interest (Table II)—possibly reflecting the larger distance adjacent fluorescent molecules have to travel to completely fill the central photobleached area. Fluorescence recovery is indeed slightly faster at the edges of the bleached area (Fig. S2 and Video 1). Importantly, filament direction and spacing were remarkably conserved over the 14-h imaging period (Fig. 4; Fig. S2). This would indicate that fluorescence recovery cannot solely be explained by rearrangement of myofibers but relates to the movement of individual titin-eGFP molecules.

Taken together, these data suggest that the titin filament system is not a rigid structure but contains a pool of titin molecules that migrate—albeit at a slower pace than other sarcomeric proteins—within the sarcomeric structure. Importantly, inhibition of protein synthesis revealed the same size of the dynamic titin pool and did not influence the mobility so that the changes in fluorescence are attributable to changes in titin mobility and not de novo synthesis of titin protein.

Longitudinal and lateral dynamics of titin-eGFP

Titin molecules are integrated into the M-band and Z-disc (Fürst et al., 1988; Wang et al., 1991; Labeit et al., 1997) and longitudinal movement along the sarcomere would require titin to disconnect, whereas lateral movement would retain titin within the half-sarcomere and merely require neighboring titin molecules to exchange positions. Conceivably, this could result in different kinetics for lateral and longitudinal diffusion of titin. To compare the mobility of titin within the myofibril (lateral movement) and between adjacent myofibrils (longitudinal movement), we followed titin movement in the photobleached area of 8 × 8 sarcomere lengths (Fig. S2; Video 1) and did not detect major differences in repopulation from lateral versus longitudinal. Furthermore, we altered the shape of the bleached area as indicated

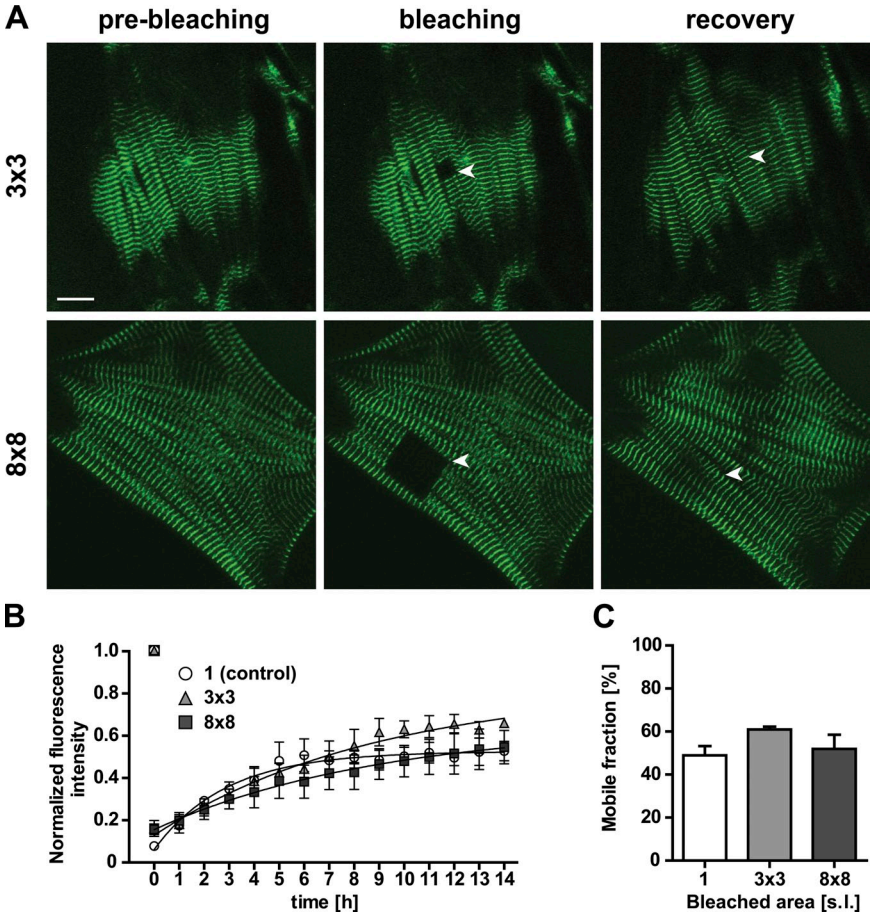

Figure 4. **Myofibril structure is maintained during FRAP.** (A) We followed fluorescence recovery in areas of 3 × 3 or 8 × 8 sarcomere lengths to distinguish movement of titin-eGFP from myofibril rearrangement. Bar, 10 µm. (B) Comparison of fluorescence recovery for 1 × 1 (control), 3 × 3, or 8 × 8 sarcomere lengths. As the region of interest increases in size recovery takes longer, emphasized in the center of the photobleached area (A, recovery at 8 × 8). (C) The mobile fractions were independent from the size of the bleached area. The recovery was homogeneous and sarcomere structure maintained over the region of interest (control, n = 4; 3 × 3, n = 4; 8 × 8, n = 3). s.l., sarcomere length. Error bars indicate SEM.

Published May 9, 2011

Table II. **Mobile fractions (M_f) and exchange half-lives ($t_{1/2}$) of titin-eGFP related to area of photobleaching**

Bleached area [s.l.]	M_f [%]	$t_{1/2}$ [h]
1 × 1	49 ± 4	2.1 ± 0.4
3 × 3	61 ± 2	6.1 ± 1.3
8 × 8	52 ± 7	8.2 ± 2.4*

s.l.: sarcomere length (n = 11).

*, $P < 0.05$; one-way ANOVA, posttest Dunnett (comparison vs. 1 × 1). Data are indicated as means ± SEM.

in Fig. 5 A with bleaching of 3 or 8 consecutive sarcomeres along or across the myofiber. Lateral and longitudinal movement were equally efficient as indicated in Fig. 5, B and C. Comparison of the mobile fractions longitudinal versus lateral for 3 sarcomeres (62 ± 5 and 58 ± 8, respectively) and longitudinal versus lateral for 8 sarcomeres (59 ± 1 and 47 ± 8, respectively) demonstrate that titin protein exchange occurs within one myofibril as well as between adjacent myofibrils at similar rates (Fig. 5, D and E). Furthermore, we found similar kinetics comparing lateral and longitudinal titin movement as indicated by the exchange half-lives of protein mobility (Fig. 5, D and E). Thus, titin mobility has more than one degree of freedom and is equally efficient along and across the sarcomere.

Calcium levels affect titin mobility

It has previously been shown that calcium does not only affect the proliferation of cardiomyocytes and protein expression, but also changes the mobility of sarcomeric proteins (Harayama et al., 1998). To investigate the effect of calcium on the mobility of titin we exposed embryonic cardiomyocytes to three different calcium concentrations (low, 0.9 mM; normal, 1.8 mM; high, 2.8 mM). Recovery was facilitated at reduced calcium levels, whereas treatment with high calcium resulted in a depressed recovery curve (Fig. 6, A and B). Differences in calcium-dependent recovery after photobleaching were largely attributable to differences in the mobile fractions, with 72 ± 4% at low calcium vs. 49 ± 4% at normal and 28 ± 5% at high calcium levels (Fig. 6 C). Calculated half-lives of titin-eGFP recovery after photobleaching were not significantly different (Table I). These data suggest that calcium levels determine the stability of titin's integration in the sarcomere, rather than the movement of titin within the myofilament. To differentiate effects of calcium mediated by myosin or contraction versus signal transduction, we used 2,3-butanedione monoxime (BDM) as a cell-permeable inhibitor of myosin II. As indicated in Fig. 7, there was no effect of BDM on titin mobility comparing beating and BDM-treated cardiomyocytes (Fig. 7, B and C). Furthermore, the effect of high calcium was not overcome by BDM treatment (Fig. 7, D and E), both arguing for a myosin- and contraction-independent effect.

Comparison of titin-eGFP mobility in embryonic and neonatal cardiomyocytes

Titin protein undergoes a perinatal isoform switch leading to the expression of shorter titin isoforms starting at the day of birth (Greaser et al., 2005). We confirmed this difference in titin isoform expression by qPCR and found a significantly higher expression of N2B in neonatal compared with embryonic cultured cardiomyocytes (Fig. S3). Together with the altered isoform expression of sarcomeric titin-binding proteins such as myomesin (Grove et al., 1985), this might have implications for retention of titin in the M-band and altered motility in embryonic versus neonatal cardiomyocytes. To investigate whether the dynamic properties of titin protein change postnatally, we performed FRAP analysis on neonatal cardiomyocytes (NCM, P2). The comparison to embryonic cardiomyocytes did not indicate any major change in fluorescence recovery of titin (Fig. 8, A and B): mobile fractions of 56 ± 3% and exchange half-lives of titin mobility (3.7 ± 0.4) were not significantly different from those calculated for embryonic cardiomyocytes (Fig. 8 C; Table I). Thus, changes in perinatal isoform expression do not exert a discernable effect on titin mobility.

Discussion

Due to titin's size and its expression in multiple isoforms it has been notoriously difficult to study the holoprotein both in vitro and in cultured cells. Circumventing the problems associated with the analysis of individual titin domains outside their native environment such as dominant-negative effects and mislocalization, researchers have used tissue- and species-specific titin isoform expression and subsequently knockout technology to gain insight into titin's roles in sarcomere assembly and stability and mechanotransduction, as well as in cardiac and skeletal muscle physiology (Weinert et al., 2006; Radke et al., 2007; Gramlich et al., 2009; Granzier et al., 2009). Based on these studies it has been proposed that titin serves as an elastic scaffold to provide both a backbone for proper assembly and localization of sarcomeric proteins and a mechanical basis for the passive functions of striated muscle (Tskhovrebova and Trinick, 2003). Earlier work has shown that the accumulation of transfected titin fragments, which consist of the Z-disc region of titin fused to GFP, leads to disassembly of the sarcomere (Turnacioglu et al., 1997). In this study, we have used the titin-eGFP knockin mouse to prevent this toxic side effect and to constitutively express titin-eGFP in cardiomyocytes at physiological levels. We asked how stable the titin scaffold is over time using the titin-eGFP mouse as a novel animal model to investigate the mobility of the titin protein. The knockin allows us to study the dynamics of titin mobility and to follow titin-eGFP's replacement after photobleaching in living cardiomyocytes.

Minimally invasive labeling of titin

Although the addition of the eGFP-tag only results in a minor addition to titin's molecular weight (<1%), we considered the possibility of steric hindrance of protein interactions and avoided manipulating titin's N terminus, which binds T-cap and is a crucial component of the Z-disc structure (Gregorio et al., 1998). Integration of titin in the M-band involves myomesin, which interacts with the Ig domain M4 (Obermann et al., 1997). There are no known interacting proteins at the very C terminus, which is thus amenable to addition of a protein tag. Indeed, the C-terminal fusion of eGFP did not affect the

Published May 9, 2011

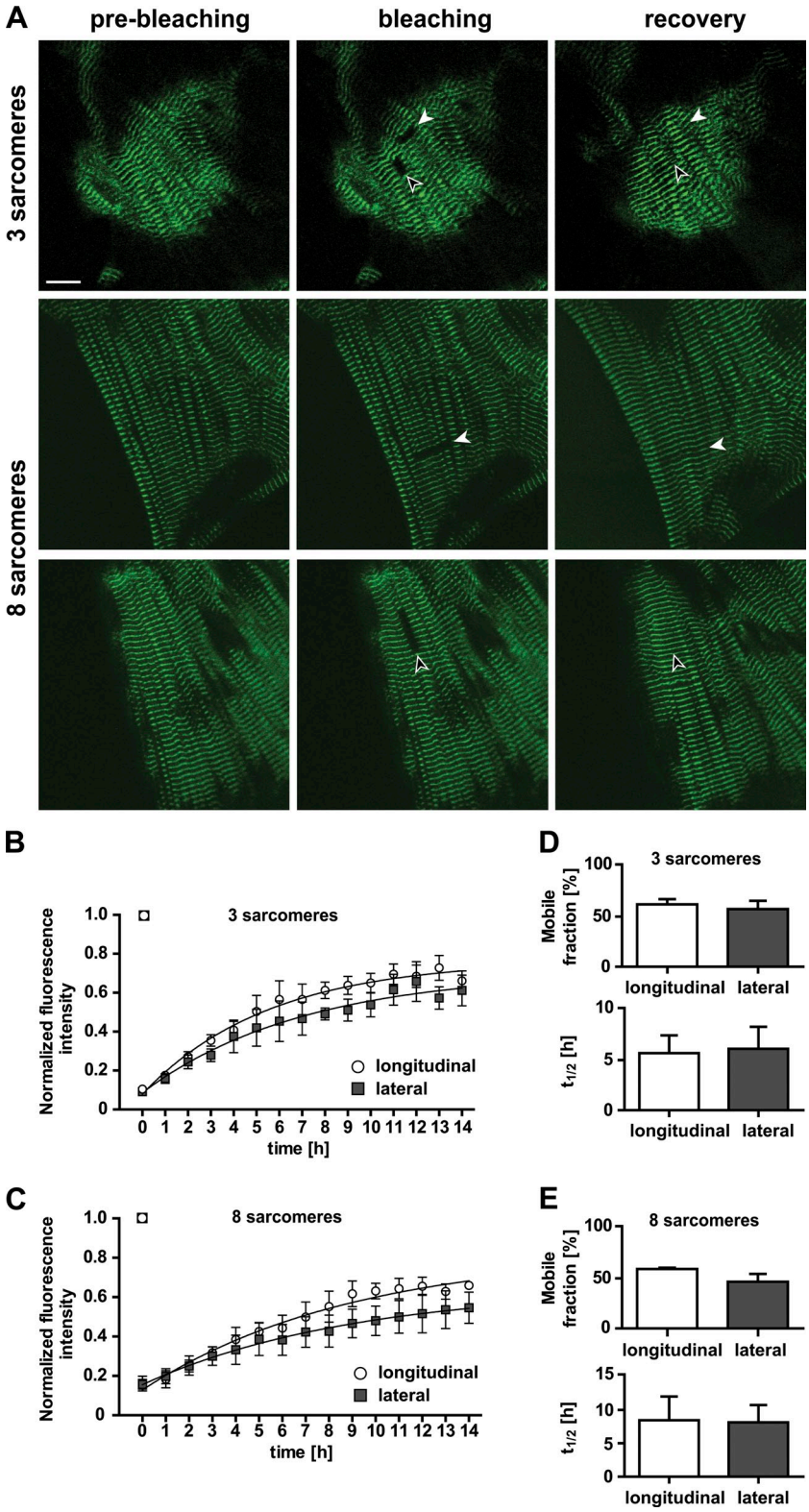

Figure 5. **Longitudinal and lateral movement of titin-eGFP within the sarcomere.** (A) Bleaching of 3 or 8 consecutive sarcomeres in embryonic cardiomyocytes was used to study longitudinal (white arrows) and lateral (open arrows) mobility of titin-eGFP. Titin-eGFP dynamics was monitored for 14 h. Bar, 10 µm. (B and C) Lateral and longitudinal movement of titin-eGFP were equally efficient as demonstrated by the plot of fluorescence intensity vs. time after photobleaching of 3 or 8 sarcomeres (3 sarcomeres, $n = 4$; 8 sarcomeres, $n = 3$). (D and E) The titin-eGFP mobile fractions were independent from the shape and area of photobleaching, whereas the half-fluorescence recovery increases with the size of the bleached area (3 sarcomeres, $n = 4$; 8 sarcomeres, $n = 3$). Error bars indicate SEM.

proper integration of titin into the M-band or sarcomere assembly and maintenance. Attaching eGFP to the C terminus only labels full-length titin, but not the shorter (up to 700 kD) novex isoforms (Bang et al., 2001). Accordingly, we specifically visualize the pool of titin isoforms that contribute to the continuous titin filament system.

Titin—more than a static scaffold

Sarcomeres are highly ordered and therefore appear as a stable structure. Nevertheless, there is a continuous movement of structural, adaptor, signaling, and metabolic proteins to and from the sarcomere. Here we examine how titin, as a protein that builds the sarcomeric backbone, is replaced and travels

Published May 9, 2011

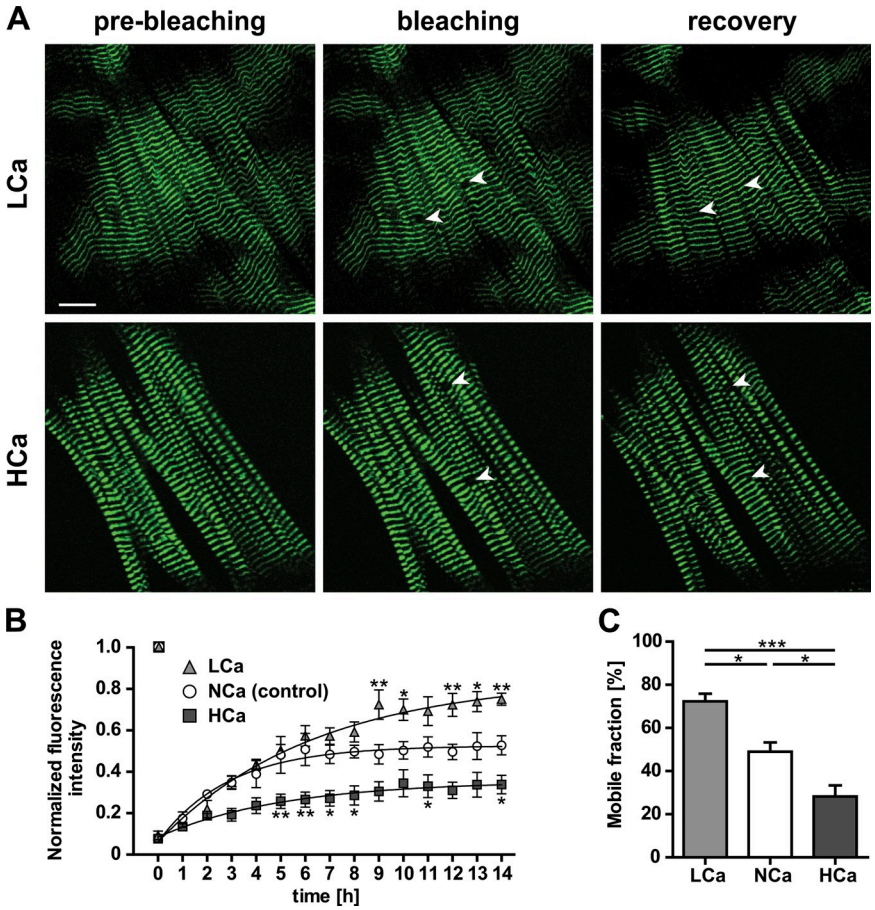

Figure 6. **Calcium interferes with titin-eGFP dynamics.** (A) Images of embryonic cardiomyocytes (E13.5) maintained at low vs. high calcium levels (0.9 mM LCa vs. 2.8 mM HCa) were obtained before and immediately after bleaching (white arrows). 14 h after bleaching the titin-eGFP signal was recovered only partially in cells treated with high as compared with low calcium. Bar, 10 µm. (B) Recovery profile of the bleached region over time. The titin-eGFP mobility was significantly increased at low calcium concentration and decreased at high calcium concentration as compared with control cells (normal, NCa, 1.8 mM; $n = 4$). (C) Mobile fractions decreased with increasing levels of calcium ($n = 4$ per group). *, $P < 0.05$; **, $P < 0.01$; ***, $P < 0.001$. Error bars indicate SEM.

within the sarcomere. It has been known for decades that the synthetic half-lives of sarcomeric proteins vary considerably and range from ∼3 to 10 d (Zak et al., 1977; Isaacs et al., 1989). These proteins are thus replaced at different rates—either within the sarcomere or after relocalization to the proteasome with a constant exchange between the sarcomeric and the cytoplasmic pool. Here, we used FRAP analysis of primary cardiomyocytes to study titin mobility. Cultured cells appeared normal, were contracting spontaneously, and remained stable throughout the photobleaching experiments. The recovery of titin-eGFP was much faster than expected based on the published synthetic half-life for newly synthesized titin protein of ∼2.9 d (Isaacs et al., 1989). We concluded that recovery after photobleaching was largely attributable to the movement of existing titin proteins within the sarcomere or cytoplasmic pool versus the integration of newly synthesized titin-eGFP protein into the sarcomere. This was confirmed by addition of CX to the media, which inhibits protein synthesis but does not significantly alter fluorescence recovery.

Sarcomere dynamics

Mobility of titin could either reflect relocalization of individual titin molecules or rearrangement of myofibrils. Although we did not detect major structural changes of the filament system in the 14-h time-lapse (compare Fig. S2 and Video 1), minor changes in location of the myofibril might occur—in part because the cells contract and also as cells shift position in culture over time. Nevertheless, we did not see a drift of the bleached area within the cell or major changes in its shape, which we would expect if fluorescence recovery was driven by rearrangement only. Based on the directionality of the sarcomere, we would expect differences in rearrangements or titin mobility along and across the myofiber, unless titin molecules are detached, relocate passively, and get reattached as outlined below.

Titin spans the half-sarcomere integrating with its N terminus into the Z-disc and with its C terminus into the M-band overlapping head-to-head and tail-to-tail (Fürst et al., 1988; Wang et al., 1991; Labeit et al., 1997). The longitudinal movement of titin along the sarcomere would therefore require titin to disconnect and reconnect in an antiparallel orientation at the succeeding next half-sarcomere. For lateral movement of titin the protein remains within the half-sarcomere with neighboring titin molecules trading places as N termini and C termini move along the Z-disc and M-band, respectively. This should be reflected in different kinetics comparing lateral and longitudinal mobility of titin-eGFP. Following the argument that an area with more lateral neighboring titin-eGFP molecules would more efficiently detect lateral movement versus an area with more longitudinal neighboring titin-eGFP, we compared laterally and longitudinally oriented regions of interest to differentiate the direction of titin mobility (Fig. 4). As regions of similar size were repopulated with similar kinetics—independent of their orientation within the cardiomyocyte—we suggest a model where titin is detached from the M-band and Z-disc and freely

Published May 9, 2011

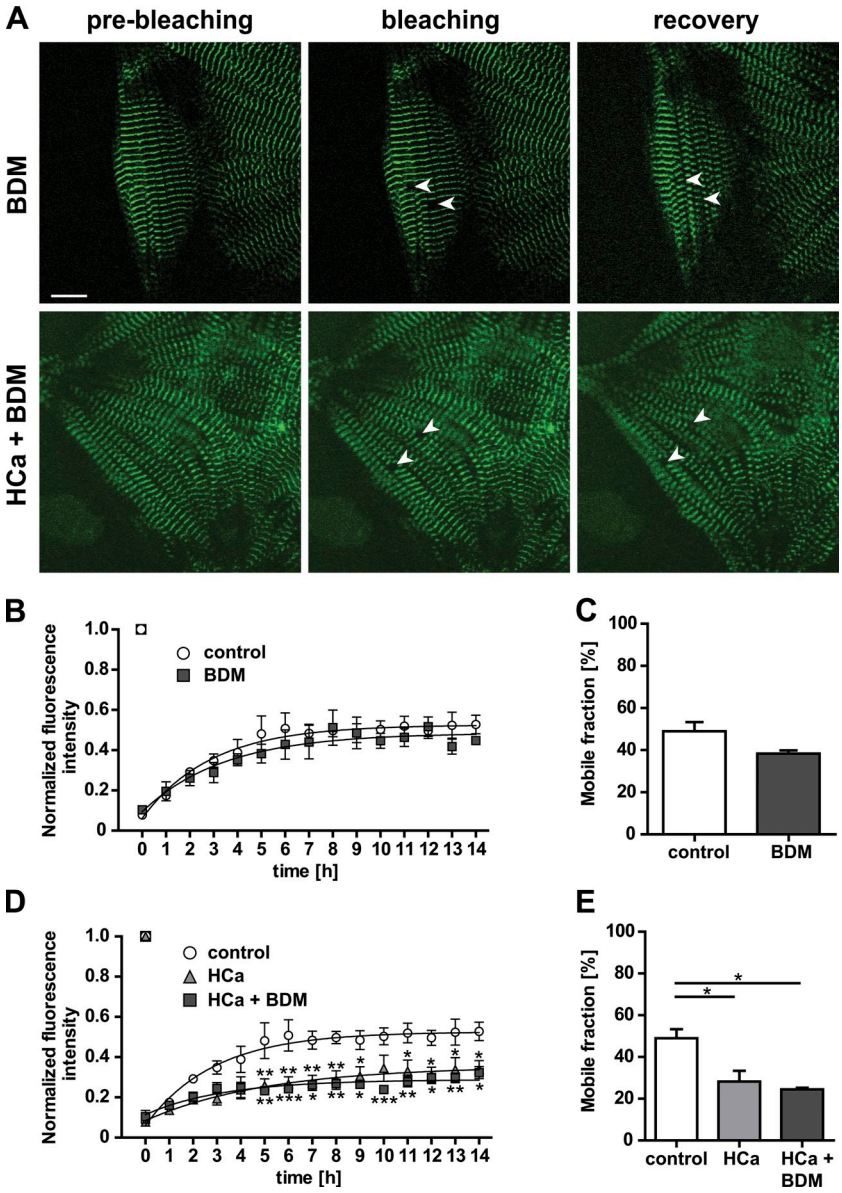

Figure 7. **Titin-eGFP dynamics in cardiomyocytes is independent from contractility.** (A) Cardiomyocytes were treated with the myosin inhibitor 2,3-butanedione monoxime (BDM), maintained in a high calcium concentration (HCa, 2.8 mM), or treated with a combination of BDM and 2.8 mM calcium. Selected regions from nonbeating cells expressing titin-eGFP were photobleached. Bar, 10 µm. (B and C) The fluorescence recovery was monitored over time. The mobility of titin-eGFP of nonbeating cells was equally efficient compared with beating control cells (control, $n = 4$; BDM, $n = 3$). (D and E) FRAP analysis with BDM treatment was repeated in cells cultured in medium with high calcium levels. The decreased dynamics of titin-eGFP could not be rescued by inhibition of contraction (control, $n = 4$; BDM + HCa, $n = 3$). *, $P < 0.05$. Error bars indicate SEM.

moves in either direction before it reintegrates. Independently, we followed recovery after photobleaching of the 8 × 8 square and found that titin-eGFP movement into the bleached area was equally efficient from either side, supporting our findings from the directional photobleaching (Fig. S2; Video 1). Thus, we would suggest that a soluble or unattached pool of titin (de novo synthesized or under migration) is distinct from a sarcomeric or attached pool of titin that is tightly integrated into the myofilament and that the unattached titin would freely move along and within the myofiber.

Calcium-dependent titin mobility

Calcium is a universal intracellular second messenger. Its multiple functions in the cardiomyocyte relate to electrophysiology, excitation–contraction coupling, contraction and relaxation, energy consumption, and cell growth and death, as well as transcriptional regulation (Bers, 2008). Toward understanding the effect of calcium on titin dynamics, it has been shown that low calcium concentrations in the culture media enhance the proliferation of cardiomyocytes and affect expression of sarcomeric proteins (Harayama et al., 1998). Within the sarcomere calcium activates contraction (Allen and Blinks, 1978) and regulates not only the interaction of actin and myosin, but also of titin and actin. High calcium levels increase the titin–actin interaction, which has been speculated to introduce a viscous force component opposing actin–myosin filament sliding (Kellermayer and Granzier, 1996; Linke et al., 2002). Furthermore, calcium binding to titin's glutamate-rich PEVK exons leads to stiffening of the PEVK element (Labeit et al., 2003; Fujita et al., 2004). These data suggest that calcium levels determine the stability of titin's integration in the sarcomere, rather than the transport of titin within the myofilament. Both the remodeling of the sarcomere with increased proliferation and the increased interaction with actin could affect titin's mobility in the sarcomere. The former would be expected to increase titin mobility as sarcomeres disassemble, the calcium-dependent increase in titin–actin interaction would conversely lead to lower motility with increased calcium levels. Our data indeed show decreased titin mobility

Published May 9, 2011

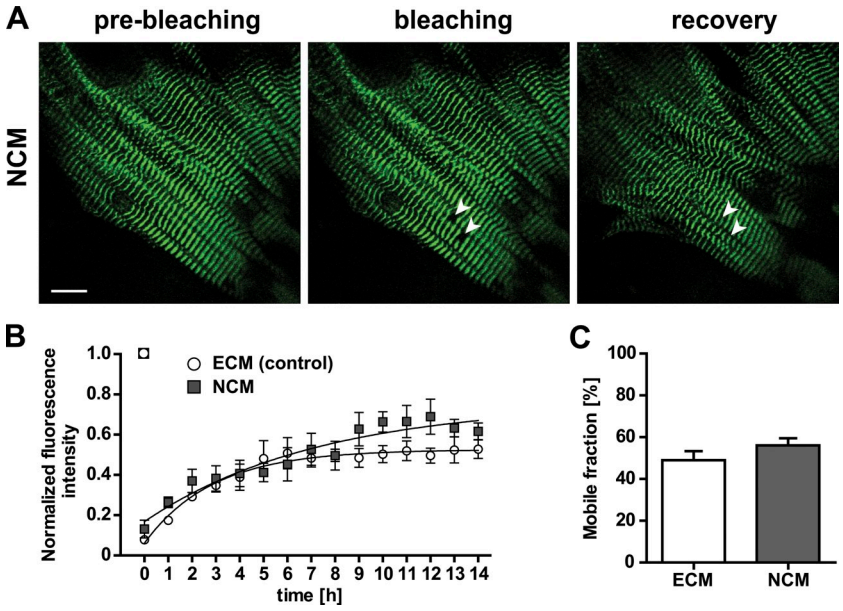

Figure 8. **Titin-eGFP dynamics in neonatal cardiomyocytes.** (A) FRAP was completed within 14 h in neonatal cardiomyocytes (NCM) prepared on postnatal day two (P2). White arrows indicate the bleached regions. Bar, 10 µm. (B) Comparison of embryonic vs. neonatal cardiomyocytes (ECM E13.5 vs. NCM P2) did not reveal a significant difference (ECM, $n = 4$; NCM, $n = 3$). (C) There was no difference in mobile fractions between neonatal and embryonic cardiomyocytes (ECM, $n = 4$; NCM, $n = 3$). Error bars indicate SEM.

with increased calcium levels that would be consistent with a stronger retention of titin at the actin filament system. Nevertheless, the calcium-dependent interaction between titin and actin is relatively weak and may suggest that the titin–actin interaction is insufficient to explain the improved FRAP at reduced calcium levels we describe here (Linke et al., 2002). Alternatively, the effect of calcium on titin motility might be mediated by altered calcium signaling and transcriptional regulation. As suitable tools become available to dissect the effects of calcium on signal transduction and protein–protein interaction, it should be possible to determine their relative contribution to stabilizing titin in the sarcomere.

Titin movement in the developing sarcomere

The pattern of cardiac protein expression changes during development and several sarcomeric proteins switch their isoform type perinatally. Thus, in rat ventricle the predominant fetal isoform β-myosin heavy chain (β-MHC) is replaced by α-MHC after birth (Lompré et al., 1984). Similarly, the α-skeletal actin isoform, which is coexpressed with α-cardiac actin before birth, is gradually replaced with the α-cardiac actin isoform in postnatal development (Carrier et al., 1992). A similar isoform switch of sarcomeric proteins has been described for troponin-I, troponin-T, tropomyosin, and the titin M-band–binding protein myomesin (Grove et al., 1985; Saggin et al., 1988, 1989; Agarkova et al., 2000; Metzger et al., 2003). Cardiac titin is intensively alternatively spliced during development and postnatally. In the embryonic mouse heart the major titin isoform is N2BA—opposed to the adult heart with mainly N2B titin and neonatal hearts, which express both isoforms (Lahmers et al., 2004; Opitz et al., 2004; Warren et al., 2004). We used FRAP of titin-eGFP knockin cardiomyocytes to evaluate if these changes in isoform expression and protein makeup of the embryonic as compared with the neonatal heart lead to altered titin dynamics. The comparison of cardiomyocytes at different stages of development did not indicate a difference in FRAP, suggesting that titin's motility is largely independent from its domain composition. Isolated adult cardiomyocytes were very sensitive to photobleaching and did not survive the FRAP procedure. Because titin displays a similar mobility in embryonic and neonatal cardiomyocytes at a time where the main changes in titin isoform expression and functional adaptation of the cardiomyocyte take place (Lahmers et al., 2004; Opitz et al., 2004; Warren et al., 2004), an additional change in the dynamics of titin in adult cardiomyocytes was not expected.

Comparative sarcomere dynamics

In FRAP experiments, the exchange of bleached by unbleached proteins occurs much faster than protein turnover would suggest, which reflects the contribution of protein movement versus de novo synthesis. Previous studies of sarcomere dynamics have shown a considerable difference in protein mobility with half-fluorescence recovery ranging from <1 to 12 min (Wang et al., 2005a), possibly related to different binding affinities or numbers of binding partners. Comparing FRAP of sarcomeric proteins allows speculation on structural functions versus a role in more dynamic processes such as signal transduction or metabolism. Within the Z-disc, the quick recovery after photobleaching of myotilin and α-actinin as compared with T-cap suggests a structural role for the latter (Wang et al., 2005a). Unlike various sarcomeric proteins studied previously, the half-fluorescence recovery of titin is in the range of hours (titin 2 h vs. T-cap ∼5 min), which further substantiates the role of titin as the sarcomeric backbone.

Actin mobility has been studied extensively with half-fluorescence recovery ranging from 1 to 60 min between β-actin in neonatal rat cardiomyocytes (Skwarek-Maruszewska et al., 2009) versus G-actin in skeletal muscle (Suzuki et al., 1998; Hasebe-Kishi and Shimada, 2000). Skeletal muscle α-actinin (rabbit) microinjected into embryonic chicken cardiomyocytes does hardly recover after photobleaching, but almost completely recovers in fibroblasts (Hasebe-Kishi and Shimada, 2000). The available literature on sarcomeric protein mobility suggests that both mobile fractions and exchange half-lives depend on the

Published May 9, 2011

species, cell type, and stage of development, although some of the variation could certainly result from experimental differences, species differences, or the amount of labeled protein after injection or overexpression. The knockin approach presented here provides the advantage of physiological levels of the labeled protein and normal regulation. Nevertheless, it is technically demanding, difficult to apply in a high throughput format, and might not provide detectable amounts of label for proteins expressed at lower levels. Titin is an ideal candidate for the knockin strategy as the locus is readily available for gene targeting and based on its robust expression in striated muscle (Weinert et al., 2006; Radke et al., 2007; Gramlich et al., 2009; Granzier et al., 2009).

Using these unique advantages, we were able to produce a tagged version of the >3 MDa titin holoprotein for live imaging and obtained novel insights into its role in sarcomere biology. We show that titin travels equally efficient along and within the myofiber—consistent with a model where titin is detached from the M-band and Z-disc and freely moves in either direction before it reintegrates into the sarcomere. Titin recovery is independent from protein synthesis and its mobility is maintained through development but inversely correlates with calcium levels. We conclude that the giant titin protein is much more dynamic than previously expected based on its size and function in the sarcomere.

Materials and methods

Generation of titin-eGFP knockin mice

A targeting construct to replace the stop codon in titin's M-band exon 6 with the eGFP cDNA (maintaining the open reading frame) was generated using standard procedures. The neomycin (Neo) resistance cassette was integrated into the 3′ untranslated region (Fig. 1). In brief, M-band exons 5 and 6 and the 3′ untranslated region were amplified from genomic DNA with suitable restriction sites included in the primer sequence. The targeting vector was assembled and verified by restriction digest and sequence analysis. Embryonic stem cells (AB1) were transfected by electroporation with the linearized targeting vector and selected with G418 as described previously (Gotthardt et al., 2003). Individual colonies were expanded and analyzed for homologous recombination by PCR and Southern blot (0.6% of neomycin resisted clones). After blastocyst injection and germline transmission, the Neo cassette was excised using the Flp FRT recombination system. Animals were backcrossed on a 129/S6 background and for each experiment littermates were used (age and sex matched).

Genotyping

Genomic DNA was prepared from mouse tail following standard procedures. Proper integration of the eGFP construct into the titin locus was monitored by PCR using primers SAK-for (5′-GCCCTTGTAAGACTTTCCAGAAT-3′) and EGFP-rev (5′-AGATGAACTTCAGGGTCAGCTTG-3′). Excision of the Neo selection marker was confirmed using primers EGFP-for (5′-GTCCTGCTGGAGTTCGTGAC-3′) and FRT-rev (5′-CAGGTCAAGTATGAAAGGATTGC-3′). The Flp recombinase allele was detected using primers Flp-for (5′-GTCACTGCAGTTTAAATACAAGACG-3′) and Flp-rev (5′-GTTGCGCTAAAGAAGTATATGTGCC-3′). Titin wild-type and titin-eGFP loci were typed using primers Mex6SAi-for (5′-AGAACAACAAGGAAGATTCCACA-3′), SAK-rev (5′-TCTCAACCCACTGAGGCATA-3′), and EGFP-rev.

Animal procedures

The body weight of age- and gender (female)-matched wild-type, heterozygous, and homozygous titin-eGFP mice was determined. Animals were sacrificed by cervical dislocation. Hearts were retrieved to calculate the heart weight to body weight ratio. All experiments involving animals were performed following the rules for Animal Welfare of the German Society for Laboratory Animal Science.

SDS-agarose electrophoresis and Western blot

Vertical SDS-agarose gel electrophoresis (VAGE) was used to detect titin-eGFP in cardiac and skeletal muscle (quadriceps and soleus) of adult knockin mice (Warren et al., 2003). For Western blot analysis the proteins were transferred to a PVDF membrane (GE Healthcare) with the PerfectBlue Semi-Dry Electroblotter SEDEC M (PEQLAB) at 250 mA for 1.5 h using anode buffer I (300 mM Tris-base, 0.05% SDS, and 10% methanol, pH 10.4), anode buffer II (25 mM Tris-base, 0.05% SDS, and 10% methanol, pH 10.4), and cathode buffer (25 mM Tris-base, 0.05% SDS, 10% methanol, 40 mM caproic acid, and 10 mM β-mercaptoethanol, pH 10.4). The membrane was blocked with blocking solution (10 mM Tris/HCl, pH 8, 150 mM NaCl, 0.1% Tween 20, 0.5% BSA, and 2.5% skim milk) followed by incubation with the polyclonal primary antibody anti-GFP (1:1,000 in blocking solution; Abcam), anti-titin Z1/Z2 (1:1,000), or anti-titin M8/M9 (1:500; Trombitás et al., 2000) at 4°C overnight. Both titin antibodies were gifts from S. Labeit (Universitätsklinikum Mannheim, Mannheim, Germany). HRP-conjugated goat anti–rabbit IgG (1:2,500 in blocking solution; Sigma-Aldrich) was used as secondary antibody. Blots were washed twice with PBS-Tween 20 followed by a PBS wash and developed by chemiluminescence staining using ECL (SuperSignal West Femto Chemiluminescent Substrate; Thermo Fisher Scientific). Images were taken using the Stella 8300 imaging system (Raytest) and processed using the Aida Image Analyzer v.2.24 software (Raytest).

Real-time PCR

Heart and skeletal muscle from adult titin-eGFP wild-type, heterozygous, and homozygous mice were used for isolation of total RNA. Primary embryonic (E13.5) and neonatal cardiomyocytes (P2) from homozygous titin-eGFP mice were cultured for 3 d and used for RNA isolation. Snap-frozen tissue was homogenized two times for 2 min at a frequency of 30/s using the TissueLyser II (QIAGEN). RNA was isolated using the peqGOLD TriFast kit (peqlab) and the RNeasy Mini kit (QIAGEN), followed by digestion of contaminating genomic DNA (RNase-Free DNase Set; QIAGEN). RNA concentration and purity were determined by spectrophotometry. 3 µg of total RNA was used for cDNA synthesis (Thermoscript First-Strand Synthesis System; Invitrogen). Quantitative real-time RT-PCR was performed using the TaqMan probe-based chemistry (Applied Biosystems). Real-time PCR amplification reaction was performed on a Sequence Detection System (7900 HT; Applied Biosystems) using the qPCR MasterMix Plus (Eurogentec) according to the manufacturer's instructions with 1x TaqMan Universal PCR master mix, 900 nM primers (EGFP-for 5′-CTGCTGCCCGACAACCAC-3′, EGFP-rev 5′-ACCATGTGATCGCGCTTCTC-3′; Mex3-4-for 5′-CCCCTGAAATTGAGTGGTTTAAA-3′, Mex3-4-rev 5′-TTCTGGAGCGACTCACACTGA-3′; Z1/Z2-for 5′-CGATGGCCGCGCTAGA-3′, Z1/Z2-rev 5′-CTCAGGGAGTATCGTCCACTGTT-3′; N2B-for 5′-GCAAAGCCTCCAATGAGTATGG-3′, N2B-rev 5′-AGGAAGTAATTTACGAACTTTCTTTTCAG-3′; N2BA-for 5′-ACAGTGGGAAAGCAAAGACATC-3′, N2BA-rev 5′-AGGTGGCCCAGAGCTACTTC-3′; endogenous control 18S RNA-for 5′-CGCCGCTAGAGGTGAAATTC-3′, 18S RNA-rev 5′-TGGGCAAATGCTTTCGCTC-3′), and 250 nM of probe (EGFP-probe 6-FAM-CCAGTCCGCCCTGAGCAAAGACC-TAMRA; Mex3-4-probe 6-FAM-AACCTTCCAATTTCCATTTCTTCA-TAMRA; Z1/Z2-probe 6-FAM-TGATGATCCCCGCCGTGACTAAAGC-TAMRA; N2B-probe 6-FAM-TGCACAGCCACACTAACTGTGACAGTGC-TAMRA; N2BA-probe 6-FAM-GAAAGAGCTGCCCCTGTGATCA-TAMRA; 18S RNA-probe 6-FAM-TGGACCGGCGCAAGACGGAC-TAMRA). Thermal cycling conditions were as follows: 50°C for 2 min, 95°C for 10 min followed by 50 cycles of 95°C for 10 s, and 60°C for 1 min. Data were collected and analyzed with Sequence Detection System 2.3 software (Applied Biosystems). The comparative CT method ($\Delta\Delta C_T$ method) was used as described in the User Bulletin 2: ABI PRISM 7700 Sequence Detection System.

Immunofluorescence staining

Adult tissues from wild-type, homozygous, and heterozygous titin-eGFP mice were dissected and used for immunofluorescence staining as described previously (Weinert et al., 2006) with the following changes. Tissues were fixed in 4% PFA for 6 h, equilibrated with 30% sucrose in PBS overnight, and embedded in Tissue Tek (O.C.T. compound; Sakura). Cryosections (5 µm) were blocked and permeabilized in blocking solution (10% goat serum, 0.3% Triton X-100, and 0.2% BSA in PBS) for 1 h. The sections were incubated with primary antibodies at 4°C overnight followed by the incubation with a biotin-conjugated antibody (1:500; BD) at room temperature for 1 h. Labeling with the fluorescent secondary antibody streptavidin A647 (1:1,000; Invitrogen) was performed at room temperature for 1 h. Primary antibodies were used at the following dilutions: 1:200 monoclonal

Published May 9, 2011

anti-sarcomeric α-actinin (Sigma-Aldrich), 1:50 anti-titin Z1/Z2, and 1:200 anti-titin M8/M9 (Trombitás et al., 2000). Fluorescence images were acquired with a laser-scanning confocal microscope (LSM 510 with software 3.2 SP2; Carl Zeiss) with a Plan-Apochromat 100x/1.4 oil DIC objective (Carl Zeiss). Images were assembled using Adobe Photoshop and Adobe Illustrator CS5.

Isolation of embryonic and neonatal murine cardiomyocytes

Timed matings were set up between homozygous animals (G/G). The morning of detection of the vaginal plug was regarded as day 0.5 after conception. Embryos were harvested at E13.5. The hearts were dissected and digested with 0.05% trypsin/EDTA (Invitrogen) for 2–4 h at 4°C followed by incubation at 37°C for 15 min. After centrifugation at 800 *g* for 3 min, the cells were resuspended in DME (Cambrex) supplemented with 10% fetal bovine serum (FBS; Sigma-Aldrich), 1% penicillin/streptomycin (Invitrogen), and 1% nonessential amino acids (Invitrogen), and plated onto 0.1% gelatin-coated plastic dishes (ibidi). The culture was maintained at 37°C and 5% CO_2 until transfer for FRAP experiments.

Neonatal (P2) hearts from homozygous titin-eGFP mice were dissected and pooled. Hearts were cut into small pieces, washed with PBS, and digested with 2.5 ml of 0.25% trypsin/EDTA (Invitrogen) at 34°C for 3 min. Trypsin solution was replaced and the tissue was incubated in 2.5 ml 0.25% trypsin/EDTA at 37°C for an additional 10 min. The supernatant was collected and the digestion was stopped with 1.25 ml of cold FBS. After centrifugation at 1,000 rpm for 8 min the pellet was resuspended in 750 µl DME and 750 µl FBS and stored on ice. The trypsinization was repeated until full digestion of the hearts. All fractions were pooled and centrifuged at 1,000 rpm for 10 min. The pellet was resuspended in DME (Cambrex) supplemented with 10% FBS, 1% penicillin/streptomycin (Invitrogen), and 1% nonessential amino acids (Invitrogen) and plated onto 0.1% gelatin-coated plastic dishes (ibidi). The culture was maintained at 37°C and 5% CO_2.

Fluorescence recovery after photobleaching and analysis of FRAP data

FRAP experiments were performed with a laser-scanning confocal microscope (LSM 510 Meta; Carl Zeiss). Titin-eGFP homozygous primary cardiomyocytes were kept at 37°C and 5% CO_2 using a CO_2 microscope cage incubation system (Okolab). For eGFP imaging the excitation wavelength and emission filters were 488 nm/band-pass 500–550 nm. Image processing was performed using LSM 510 Image Browser version 4.2 (Carl Zeiss). For FRAP experiments a Plan-Apochromat 63x/1.4 oil Ph3 objective was used and the confocal pinhole was set to 1.5 µm. 3–4 experiments (n = 3–4) were performed and each time 4–10 cells were selected. For every cell 1 or 2 different regions of interest (ROI) were chosen for bleaching to keep phototoxicity low and areas of interest were limited to squares of 1, 3, or 8 sarcomere lengths or areas of 1 sarcomere length × 3 or 8 sarcomere lengths along or across the myofiber. Images were taken before and immediately after bleaching. Photobleaching was done with 100% intensity of the 488-nm laser for 20 iterations. The fluorescence recovery was monitored 14 times every hour and measured using the LSM Image Examiner (Carl Zeiss). Normalized FRAP curves were generated from raw data as described in Al Tanoury et al. (2010). Background intensity ($I_{base}(t)$) was measured in a region outside of the cell and then subtracted from the intensity of the bleached area ($I_{frap}(t)$) and the whole cell ($I_{whole}(t)$) at each time point. The intensities were then normalized by rescaling to the prebleach intensities in the corresponding regions ($I_{frap\text{-}pre}$, and $I_{whole\ pre}$). The resulting equation for the normalized FRAP curve is:

$$I_{frap-norm}(t) = \frac{I_{frap}(t) - I_{base}(t)}{I_{whole}(t) - I_{base}(t)} * \frac{I_{whole-pre}}{I_{frap-pre}} . \quad (1)$$

To obtain the exchange half-life ($t_{1/2}$) data were displayed as normalized fluorescence intensity versus time using Prism 5.0 (GraphPad Software). The model of one phase association was applied to fit the data:

$$y(t) = (y_0 + Mf) * (1 - e^{(1-K*x)}) . \quad (2)$$

The fluorescence intensity at time zero after bleaching is defined as y_0. K is the rate constant. The exchange half-life ($t_{1/2}$) is computed as follows:

$$t_{1/2} = \frac{\ln(2)}{K} . \quad (3)$$

M_f is the mobile fraction and is calculated with the following equation:

$$Mf = \frac{F_{end} - F_{post}}{F_{pre} - F_{post}} . \quad (4)$$

F_{end} is the fluorescence intensity when the recovery has reached the plateau level. F_{pre} is defined as the fluorescence intensity before and F_{post} after photobleaching. FRAP data are displayed as mean of 3–4 individual experiments.

Cycloheximide, calcium, and BDM treatment

Cycloheximide (CX; Sigma-Aldrich) is a general inhibitor of protein synthesis that blocks elongation of translation. 10 µg/ml of CX were included in the media. Cells were incubated in CX for 1 h before and during the FRAP experiment (Zaal et al., 1999).

The role of calcium on the FRAP was evaluated by various calcium concentrations in the culture medium as described in Harayama et al. (1998). In short, embryonic cardiomyocytes were isolated and after preculture for 3 d 0.9 mM (low, LCa), 1.8 mM (normal, NCa; control), or 2.8 mM (high, HCa) of calcium were added to the culture medium. The treatment was repeated after 2 d. On the fifth day of treatment the cells were used for FRAP analysis.

To differentiate an effect of calcium on signaling or protein binding versus contraction, we treated cardiomyocytes with the myosin inhibitor 2,3-butanedione monoxime (BDM; Sigma-Aldrich). FRAP experiments were performed 15 min after addition of 15 mM BDM, when cells had stopped beating.

Statistical analysis

Differences between two groups were assessed by *t* test and between three groups by one-way ANOVA. Groups affected by two factors were assessed by two-way ANOVA. For statistical analysis we used Prism 5.0 (GraphPad Software). Significance was set at a probability value of 0.05. All results are expressed as mean ± SEM.

Online supplemental material

Fig. S1 shows Western blot analysis of the expression of titin-eGFP in striated muscle. Fig. S2 provides time-lapse images documenting the fluorescence recovery of titin-eGFP in a larger bleached area. Fig. S3 confirms the differences in titin isoform expression in neonatal as compared with embryonic cardiomyocytes. Video 1 is a time-lapse video showing the FRAP analysis of titin-eGFP in a larger bleached area. Online supplemental material is available at http://www.jcb.org/cgi/content/full/jcb.201010099/DC1.

The authors thank Beate Golbrich-Hannig and Carolin Gärtner for expert technical assistance and Siegfried Labeit for the anti-titin antibodies. We also thank Anje Sporbert and Zoltan Cseresnyes from the Microscope Core Facility of the MDC for technical support.

This work was supported by the DFG, the Alexander von Humboldt Foundation, and the Thyssen Foundation (to M. Gotthardt).

Submitted: 20 October 2010
Accepted: 6 April 2011

References

Agarkova, I., D. Auerbach, E. Ehler, and J.C. Perriard. 2000. A novel marker for vertebrate embryonic heart, the EH-myomesin isoform. *J. Biol. Chem.* 275:10256–10264. doi:10.1074/jbc.275.14.10256

Al Tanoury, Z., E. Schaffner-Reckinger, A. Halavatyi, C. Hoffmann, M. Moes, E. Hadzic, M. Catillon, M. Yatskou, and E. Friederich. 2010. Quantitative kinetic study of the actin-bundling protein L-plastin and of its impact on actin turn-over. *PLoS ONE*. 5:e9210. doi:10.1371/journal.pone.0009210

Allen, D.G., and J.R. Blinks. 1978. Calcium transients in aequorin-injected frog cardiac muscle. *Nature*. 273:509–513. doi:10.1038/273509a0

Bähler, M., T. Wallimann, and H.M. Eppenberger. 1985. Myofibrillar M-band proteins represent constituents of native thick filaments, frayed filaments and bare zone assemblages. *J. Muscle Res. Cell Motil.* 6:783–800. doi:10.1007/BF00712242

Bang, M.L., T. Centner, F. Fornoff, A.J. Geach, M. Gotthardt, M. McNabb, C.C. Witt, D. Labeit, C.C. Gregorio, H. Granzier, and S. Labeit. 2001. The complete gene sequence of titin, expression of an unusual approximately 700-kDa titin isoform, and its interaction with obscurin identify a novel Z-line to I-band linking system. *Circ. Res.* 89:1065–1072. doi:10.1161/hh2301.100981

Bers, D.M. 2008. Calcium cycling and signaling in cardiac myocytes. *Annu. Rev. Physiol.* 70:23–49. doi:10.1146/annurev.physiol.70.113006.100455

Carrier, L., K.R. Boheler, C. Chassagne, D. de la Bastie, C. Wisnewsky, E.G. Lakatta, and K. Schwartz. 1992. Expression of the sarcomeric actin isogenes in the rat heart with development and senescence. *Circ. Res.* 70:999–1005.

Centner, T., J. Yano, E. Kimura, A.S. McElhinny, K. Pelin, C.C. Witt, M.L. Bang, K. Trombitas, H. Granzier, C.C. Gregorio, et al. 2001. Identification of muscle specific ring finger proteins as potential regulators of the titin kinase domain. *J. Mol. Biol.* 306:717–726. doi:10.1006/jmbi.2001.4448

Dabiri, G.A., K.K. Turnacioglu, J.M. Sanger, and J.W. Sanger. 1997. Myofibrillogenesis visualized in living embryonic cardiomyocytes. *Proc. Natl. Acad. Sci. USA*. 94:9493–9498. doi:10.1073/pnas.94.17.9493

Dome, J.S., B. Mittal, M.B. Pochapin, J.M. Sanger, and J.W. Sanger. 1988. Incorporation of fluorescently labeled actin and tropomyosin into muscle cells. *Cell Differ.* 23:37–52. doi:10.1016/0045-6039(88)90035-8

Du, A., J.M. Sanger, K.K. Linask, and J.W. Sanger. 2003. Myofibrillogenesis in the first cardiomyocytes formed from isolated quail precardiac mesoderm. *Dev. Biol.* 257:382–394. doi:10.1016/S0012-1606(03)00104-0

Freiburg, A., and M. Gautel. 1996. A molecular map of the interactions between titin and myosin-binding protein C. Implications for sarcomeric assembly in familial hypertrophic cardiomyopathy. *Eur. J. Biochem.* 235:317–323. doi:10.1111/j.1432-1033.1996.00317.x

Fujita, H., D. Labeit, B. Gerull, S. Labeit, and H.L. Granzier. 2004. Titin isoform-dependent effect of calcium on passive myocardial tension. *Am. J. Physiol. Heart Circ. Physiol.* 287:H2528–H2534. doi:10.1152/ajpheart.00553.2004

Fürst, D.O., M. Osborn, R. Nave, and K. Weber. 1988. The organization of titin filaments in the half-sarcomere revealed by monoclonal antibodies in immunoelectron microscopy: a map of ten nonrepetitive epitopes starting at the Z line extends close to the M line. *J. Cell Biol.* 106:1563–1572. doi:10.1083/jcb.106.5.1563

Fürst, D.O., M. Osborn, and K. Weber. 1989. Myogenesis in the mouse embryo: differential onset of expression of myogenic proteins and the involvement of titin in myofibril assembly. *J. Cell Biol.* 109:517–527. doi:10.1083/jcb.109.2.517

Gotthardt, M., R.E. Hammer, N. Hübner, J. Monti, C.C. Witt, M. McNabb, J.A. Richardson, H. Granzier, S. Labeit, and J. Herz. 2003. Conditional expression of mutant M-line titins results in cardiomyopathy with altered sarcomere structure. *J. Biol. Chem.* 278:6059–6065. doi:10.1074/jbc.M211723200

Gramlich, M., B. Michely, C. Krohne, A. Heuser, B. Erdmann, S. Klaassen, B. Hudson, M. Magarin, F. Kirchner, M. Todiras, et al. 2009. Stress-induced dilated cardiomyopathy in a knock-in mouse model mimicking human titin-based disease. *J. Mol. Cell. Cardiol.* 47:352–358. doi:10.1016/j.yjmcc.2009.04.014

Granzier, H.L., M.H. Radke, J. Peng, D. Westermann, O.L. Nelson, K. Rost, N.M.P. King, Q. Yu, C. Tschöpe, M. McNabb, et al. 2009. Truncation of titin's elastic PEVK region leads to cardiomyopathy with diastolic dysfunction. *Circ. Res.* 105:557–564. doi:10.1161/CIRCRESAHA.109.200964

Greaser, M.L., P.R. Krzesinski, C.M. Warren, B. Kirkpatrick, K.S. Campbell, and R.L. Moss. 2005. Developmental changes in rat cardiac titin/connectin: transitions in normal animals and in mutants with a delayed pattern of isoform transition. *J. Muscle Res. Cell Motil.* 26:325–332. doi:10.1007/s10974-005-9039-0

Gregorio, C.C., K. Trombitás, T. Centner, B. Kolmerer, G. Stier, K. Kunke, K. Suzuki, F. Obermayr, B. Herrmann, H. Granzier, et al. 1998. The NH2 terminus of titin spans the Z-disc: its interaction with a novel 19-kD ligand (T-cap) is required for sarcomeric integrity. *J. Cell Biol.* 143:1013–1027. doi:10.1083/jcb.143.4.1013

Grove, B.K., L. Cerny, J.C. Perriard, and H.M. Eppenberger. 1985. Myomesin and M-protein: expression of two M-band proteins in pectoral muscle and heart during development. *J. Cell Biol.* 101:1413–1421. doi:10.1083/jcb.101.4.1413

Harayama, H., M. Koide, K. Obata, A. Iio, M. Iida, N. Matsuda, R.E. Akins, M. Yokota, R.S. Tuan, and H. Saito. 1998. Influence of calcium on proliferation and phenotype alteration of cardiomyocyte in vitro. *J. Cell. Physiol.* 177:289–298. doi:10.1002/(SICI)1097-4652(199811)177:2<289::AID-JCP11>3.0.CO;2-5

Hasebe-Kishi, F., and Y. Shimada. 2000. Dynamics of actin and alpha-actinin in nascent myofibrils and stress fibers. *J. Muscle Res. Cell Motil.* 21:717–724. doi:10.1023/A:1010374424143

Houmeida, A., J. Holt, L. Tskhovrebova, and J. Trinick. 1995. Studies of the interaction between titin and myosin. *J. Cell Biol.* 131:1471–1481. doi:10.1083/jcb.131.6.1471

Isaacs, W.B., I.S. Kim, A. Struve, and A.B. Fulton. 1989. Biosynthesis of titin in cultured skeletal muscle cells. *J. Cell Biol.* 109:2189–2195. doi:10.1083/jcb.109.5.2189

Kellermayer, M.S., and H.L. Granzier. 1996. Calcium-dependent inhibition of in vitro thin-filament motility by native titin. *FEBS Lett.* 380:281–286. doi:10.1016/0014-5793(96)00055-5

Kinbara, K., H. Sorimachi, S. Ishiura, and K. Suzuki. 1997. Muscle-specific calpain, p94, interacts with the extreme C-terminal region of connectin, a unique region flanked by two immunoglobulin C2 motifs. *Arch. Biochem. Biophys.* 342:99–107. doi:10.1006/abbi.1997.0108

Kramerova, I., E. Kudryashova, J.G. Tidball, and M.J. Spencer. 2004. Null mutation of calpain 3 (p94) in mice causes abnormal sarcomere formation in vivo and in vitro. *Hum. Mol. Genet.* 13:1373–1388. doi:10.1093/hmg/ddh153

Kulke, M., S. Fujita-Becker, E. Rostkova, C. Neagoe, D. Labeit, D.J. Manstein, M. Gautel, and W.A. Linke. 2001. Interaction between PEVK-titin and actin filaments: origin of a viscous force component in cardiac myofibrils. *Circ. Res.* 89:874–881. doi:10.1161/hh2201.099453

Labeit, S., and B. Kolmerer. 1995. Titins: giant proteins in charge of muscle ultra structure and elasticity. *Science*. 270:293–296. doi:10.1126/science.270.5234.293

Labeit, S., M. Gautel, A. Lakey, and J. Trinick. 1992. Towards a molecular understanding of titin. *EMBO J.* 11:1711–1716.

Labeit, S., B. Kolmerer, and W.A. Linke. 1997. The giant protein titin. Emerging roles in physiology and pathophysiology. *Circ. Res.* 80:290–294.

Labeit, D., K. Watanabe, C. Witt, H. Fujita, Y. Wu, S. Lahmers, T. Funck, S. Labeit, and H. Granzier. 2003. Calcium-dependent molecular spring elements in the giant protein titin. *Proc. Natl. Acad. Sci. USA*. 100:13716–13721. doi:10.1073/pnas.2235652100

Lahmers, S., Y. Wu, D.R. Call, S. Labeit, and H. Granzier. 2004. Developmental control of titin isoform expression and passive stiffness in fetal and neonatal myocardium. *Circ. Res.* 94:505–513. doi:10.1161/01.RES.0000115522.52554.86

Lange, S., D. Auerbach, P. McLoughlin, E. Perriard, B.W. Schäfer, J.C. Perriard, and E. Ehler. 2002. Subcellular targeting of metabolic enzymes to titin in heart muscle may be mediated by DRAL/FHL-2. *J. Cell Sci.* 115:4925–4936. doi:10.1242/jcs.00181

Linke, W.A., M. Kulke, H. Li, S. Fujita-Becker, C. Neagoe, D.J. Manstein, M. Gautel, and J.M. Fernandez. 2002. PEVK domain of titin: an entropic spring with actin-binding properties. *J. Struct. Biol.* 137:194–205. doi:10.1006/jsbi.2002.4468

Lompré, A.M., B. Nadal-Ginard, and V. Mahdavi. 1984. Expression of the cardiac ventricular alpha- and beta-myosin heavy chain genes is developmentally and hormonally regulated. *J. Biol. Chem.* 259:6437–6446.

Makarenko, I., C.A. Opitz, M.C. Leake, C. Neagoe, M. Kulke, J.K. Gwathmey, F. del Monte, R.J. Hajjar, and W.A. Linke. 2004. Passive stiffness changes caused by upregulation of compliant titin isoforms in human dilated cardiomyopathy hearts. *Circ. Res.* 95:708–716. doi:10.1161/01.RES.0000143901.37063.2f

McElhinny, A.S., K. Kakinuma, H. Sorimachi, S. Labeit, and C.C. Gregorio. 2002. Muscle-specific RING finger-1 interacts with titin to regulate sarcomeric M-line and thick filament structure and may have nuclear functions via its interaction with glucocorticoid modulatory element binding protein-1. *J. Cell Biol.* 157:125–136. doi:10.1083/jcb.200108089

McKenna, N., J.B. Meigs, and Y.L. Wang. 1985a. Identical distribution of fluorescently labeled brain and muscle actins in living cardiac fibroblasts and myocytes. *J. Cell Biol.* 100:292–296. doi:10.1083/jcb.100.1.292

McKenna, N.M., J.B. Meigs, and Y.L. Wang. 1985b. Exchangeability of alpha-actinin in living cardiac fibroblasts and muscle cells. *J. Cell Biol.* 101:2223–2232. doi:10.1083/jcb.101.6.2223

Metzger, J.M., D.E. Michele, E.M. Rust, A.R. Borton, and M.V. Westfall. 2003. Sarcomere thin filament regulatory isoforms. Evidence of a dominant effect of slow skeletal troponin I on cardiac contraction. *J. Biol. Chem.* 278:13118–13123. doi:10.1074/jbc.M212601200

Miller, M.K., M.L. Bang, C.C. Witt, D. Labeit, C. Trombitas, K. Watanabe, H. Granzier, A.S. McElhinny, C.C. Gregorio, and S. Labeit. 2003. The muscle ankyrin repeat proteins: CARP, ankrd2/Arpp and DARP as a family of titin filament-based stress response molecules. *J. Mol. Biol.* 333:951–964. doi:10.1016/j.jmb.2003.09.012

Mittal, B., J.M. Sanger, and J.W. Sanger. 1987. Visualization of myosin in living cells. *J. Cell Biol.* 105:1753–1760. doi:10.1083/jcb.105.4.1753

Nave, R., D.O. Fürst, and K. Weber. 1989. Visualization of the polarity of isolated titin molecules: a single globular head on a long thin rod as the M band anchoring domain? *J. Cell Biol.* 109:2177–2187. doi:10.1083/jcb.109.5.2177

Neagoe, C., M. Kulke, F. del Monte, J.K. Gwathmey, P.P. de Tombe, R.J. Hajjar, and W.A. Linke. 2002. Titin isoform switch in ischemic human heart disease. *Circulation*. 106:1333–1341. doi:10.1161/01.CIR.0000029803.93022.93

Obermann, W.M., M. Gautel, F. Steiner, P.F. van der Ven, K. Weber, and D.O. Fürst. 1996. The structure of the sarcomeric M band: localization of defined

domains of myomesin, M-protein, and the 250-kD carboxy-terminal region of titin by immunoelectron microscopy. *J. Cell Biol.* 134:1441–1453. doi:10.1083/jcb.134.6.1441

Obermann, W.M., M. Gautel, K. Weber, and D.O. Fürst. 1997. Molecular structure of the sarcomeric M band: mapping of titin and myosin binding domains in myomesin and the identification of a potential regulatory phosphorylation site in myomesin. *EMBO J.* 16:211–220. doi:10.1093/emboj/16.2.211

Ohtsuka, H., H. Yajima, K. Maruyama, and S. Kimura. 1997a. Binding of the N-terminal 63 kDa portion of connectin/titin to alpha-actinin as revealed by the yeast two-hybrid system. *FEBS Lett.* 401:65–67. doi:10.1016/S0014-5793(96)01432-9

Ohtsuka, H., H. Yajima, K. Maruyama, and S. Kimura. 1997b. The N-terminal Z repeat 5 of connectin/titin binds to the C-terminal region of alpha-actinin. *Biochem. Biophys. Res. Commun.* 235:1–3. doi:10.1006/bbrc.1997.6534

Opitz, C.A., M.C. Leake, I. Makarenko, V. Benes, and W.A. Linke. 2004. Developmentally regulated switching of titin size alters myofibrillar stiffness in the perinatal heart. *Circ. Res.* 94:967–975. doi:10.1161/01.RES.0000124301.48193.E1

Pizon, V., A. Iakovenko, P.F. Van Der Ven, R. Kelly, C. Fatu, D.O. Fürst, E. Karsenti, and M. Gautel. 2002. Transient association of titin and myosin with microtubules in nascent myofibrils directed by the MURF2 RING-finger protein. *J. Cell Sci.* 115:4469–4482. doi:10.1242/jcs.00131

Radke, M.H., J. Peng, Y. Wu, M. McNabb, O.L. Nelson, H. Granzier, and M. Gotthardt. 2007. Targeted deletion of titin N2B region leads to diastolic dysfunction and cardiac atrophy. *Proc. Natl. Acad. Sci. USA*. 104:3444–3449. doi:10.1073/pnas.0608543104

Rhee, D., J.M. Sanger, and J.W. Sanger. 1994. The premyofibril: evidence for its role in myofibrillogenesis. *Cell Motil. Cytoskeleton*. 28:1–24. doi:10.1002/cm.970280102

Saggin, L., S. Ausoni, L. Gorza, S. Sartore, and S. Schiaffino. 1988. Troponin T switching in the developing rat heart. *J. Biol. Chem.* 263:18488–18492.

Saggin, L., L. Gorza, S. Ausoni, and S. Schiaffino. 1989. Troponin I switching in the developing heart. *J. Biol. Chem.* 264:16299–16302.

Sanger, J.M., B. Mittal, M.B. Pochapin, and J.W. Sanger. 1986. Myofibrillogenesis in living cells microinjected with fluorescently labeled alpha-actinin. *J. Cell Biol.* 102:2053–2066. doi:10.1083/jcb.102.6.2053

Sanger, J.W., J.C. Ayoob, P. Chowrashi, D. Zurawski, and J.M. Sanger. 2000. Assembly of myofibrils in cardiac muscle cells. *Adv. Exp. Med. Biol.* 481:89–102, discussion :103–105.

Sanger, J.W., J. Wang, B. Holloway, A. Du, and J.M. Sanger. 2009. Myofibrillogenesis in skeletal muscle cells in zebrafish. *Cell Motil. Cytoskeleton*. 66:556–566. doi:10.1002/cm.20365

Schaart, G., C. Viebahn, W. Langmann, and F. Ramaekers. 1989. Desmin and titin expression in early postimplantation mouse embryos. *Development*. 107:585–596.

Skwarek-Maruszewska, A., P. Hotulainen, P.K. Mattila, and P. Lappalainen. 2009. Contractility-dependent actin dynamics in cardiomyocyte sarcomeres. *J. Cell Sci.* 122:2119–2126. doi:10.1242/jcs.046805

Sorimachi, H., K. Kinbara, S. Kimura, M. Takahashi, S. Ishiura, N. Sasagawa, N. Sorimachi, H. Shimada, K. Tagawa, K. Maruyama, et al. 1995. Muscle-specific calpain, p94, responsible for limb girdle muscular dystrophy type 2A, associates with connectin through IS2, a p94-specific sequence. *J. Biol. Chem.* 270:31158–31162. doi:10.1074/jbc.270.13.7437

Sorimachi, H., A. Freiburg, B. Kolmerer, S. Ishiura, G. Stier, C.C. Gregorio, D. Labeit, W.A. Linke, K. Suzuki, and S. Labeit. 1997. Tissue-specific expression and alpha-actinin binding properties of the Z-disc titin: implications for the nature of vertebrate Z-discs. *J. Mol. Biol.* 270:688–695. doi:10.1006/jmbi.1997.1145

Stahlhut, M., J.S. Petersen, J.K. Hennan, and M.T. Ramirez. 2006. The anti-arrhythmic peptide rotigaptide (ZP123) increases connexin 43 protein expression in neonatal rat ventricular cardiomyocytes. *Cell Commun. Adhes.* 13:21–27. doi:10.1080/15419060600631375

Stout, A.L., J. Wang, J.M. Sanger, and J.W. Sanger. 2008. Tracking changes in Z-band organization during myofibrillogenesis with FRET imaging. *Cell Motil. Cytoskeleton*. 65:353–367. doi:10.1002/cm.20265

Suzuki, H., M. Komiyama, A. Konno, and Y. Shimada. 1998. Exchangeability of actin in cardiac myocytes and fibroblasts as determined by fluorescence photobleaching recovery. *Tissue Cell*. 30:274–280. doi:10.1016/S0040-8166(98)80076-1

Trinick, J. 1996. Titin as a scaffold and spring. Cytoskeleton. *Curr. Biol.* 6:258–260. doi:10.1016/S0960-9822(02)00472-4

Trombitás, K., A. Freiburg, M. Greaser, S. Labeit, and H. Granzier. 2000. From connecting filaments to co-expression of titin isoforms. *Adv. Exp. Med. Biol.* 481:405–418.

Tskhovrebova, L., and J. Trinick. 2003. Titin: properties and family relationships. *Nat. Rev. Mol. Cell Biol.* 4:679–689. doi:10.1038/nrm1198

Turnacioglu, K.K., B. Mittal, G.A. Dabiri, J.M. Sanger, and J.W. Sanger. 1997. An N-terminal fragment of titin coupled to green fluorescent protein localizes to the Z-bands in living muscle cells: overexpression leads to myofibril disassembly. *Mol. Biol. Cell*. 8:705–717.

van der Loop, F.T., P.F. van der Ven, D.O. Fürst, M. Gautel, G.J. van Eys, and F.C. Ramaekers. 1996. Integration of titin into the sarcomeres of cultured differentiating human skeletal muscle cells. *Eur. J. Cell Biol.* 69:301–307.

Vinkemeier, U., W. Obermann, K. Weber, and D.O. Fürst. 1993. The globular head domain of titin extends into the center of the sarcomeric M band. cDNA cloning, epitope mapping and immunoelectron microscopy of two titin-associated proteins. *J. Cell Sci.* 106:319–330.

Wang, S.M., M.C. Sun, and C.J. Jeng. 1991. Location of the C-terminus of titin at the Z-line region in the sarcomere. *Biochem. Biophys. Res. Commun.* 176:189–193. doi:10.1016/0006-291X(91)90907-O

Wang, J., N. Shaner, B. Mittal, Q. Zhou, J. Chen, J.M. Sanger, and J.W. Sanger. 2005a. Dynamics of Z-band based proteins in developing skeletal muscle cells. *Cell Motil. Cytoskeleton*. 61:34–48. doi:10.1002/cm.20063

Wang, J., J.M. Sanger, and J.W. Sanger. 2005b. Differential effects of Latrunculin-A on myofibrils in cultures of skeletal muscle cells: insights into mechanisms of myofibrillogenesis. *Cell Motil. Cytoskeleton*. 62:35–47. doi:10.1002/cm.20083

Warren, C.M., P.R. Krzesinski, and M.L. Greaser. 2003. Vertical agarose gel electrophoresis and electroblotting of high-molecular-weight proteins. *Electrophoresis*. 24:1695–1702. doi:10.1002/elps.200305392

Warren, C.M., P.R. Krzesinski, K.S. Campbell, R.L. Moss, and M.L. Greaser. 2004. Titin isoform changes in rat myocardium during development. *Mech. Dev.* 121:1301–1312. doi:10.1016/j.mod.2004.07.003

Weinert, S., N. Bergmann, X. Luo, B. Erdmann, and M. Gotthardt. 2006. M line-deficient titin causes cardiac lethality through impaired maturation of the sarcomere. *J. Cell Biol.* 173:559–570. doi:10.1083/jcb.200601014

Witt, S.H., H. Granzier, C.C. Witt, and S. Labeit. 2005. MURF-1 and MURF-2 target a specific subset of myofibrillar proteins redundantly: towards understanding MURF-dependent muscle ubiquitination. *J. Mol. Biol.* 350:713–722. doi:10.1016/j.jmb.2005.05.021

Yamasaki, R., M. Berri, Y. Wu, K. Trombitás, M. McNabb, M.S. Kellermayer, C. Witt, D. Labeit, S. Labeit, M. Greaser, and H. Granzier. 2001. Titin-actin interaction in mouse myocardium: passive tension modulation and its regulation by calcium/S100A1. *Biophys. J.* 81:2297–2313. doi:10.1016/S0006-3495(01)75876-6

Zaal, K.J., C.L. Smith, R.S. Polishchuk, N. Altan, N.B. Cole, J. Ellenberg, K. Hirschberg, J.F. Presley, T.H. Roberts, E. Siggia, et al. 1999. Golgi membranes are absorbed into and reemerge from the ER during mitosis. *Cell*. 99:589–601. doi:10.1016/S0092-8674(00)81548-2

Zak, R., A.F. Martin, G. Prior, and M. Rabinowitz. 1977. Comparison of turnover of several myofibrillar proteins and critical evaluation of double isotope method. *J. Biol. Chem.* 252:3430–3435.

Zou, P., N. Pinotsis, S. Lange, Y.H. Song, A. Popov, I. Mavridis, O.M. Mayans, M. Gautel, and M. Wilmanns. 2006. Palindromic assembly of the giant muscle protein titin in the sarcomeric Z-disk. *Nature*. 439:229–233. doi:10.1038/nature04343

Published May 9, 2011

da Silva Lopes et al., http://www.jcb.org/cgi/content/full/jcb.201010099/DC1

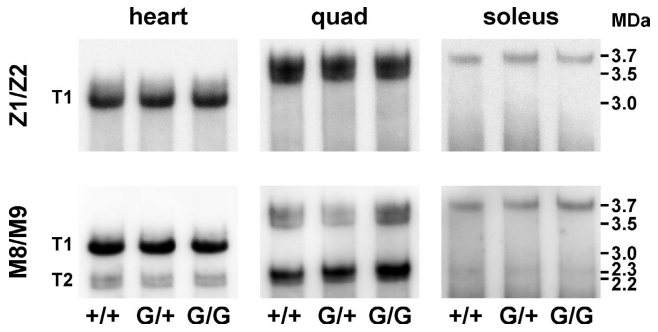

Figure S1. **Analysis of titin-eGFP protein expression in striated muscle.** Western blot analysis of titin in wild-type (+/+), heterozygous (G/+), and homozygous (G/G) heart, quadriceps, and soleus using antibodies directed against titin's Z-disc region Z1/Z2 and M-band region M8/M9. There were no differences in titin protein levels between genotypes. T1, full length titin; T2, degradation product.

Published May 9, 2011

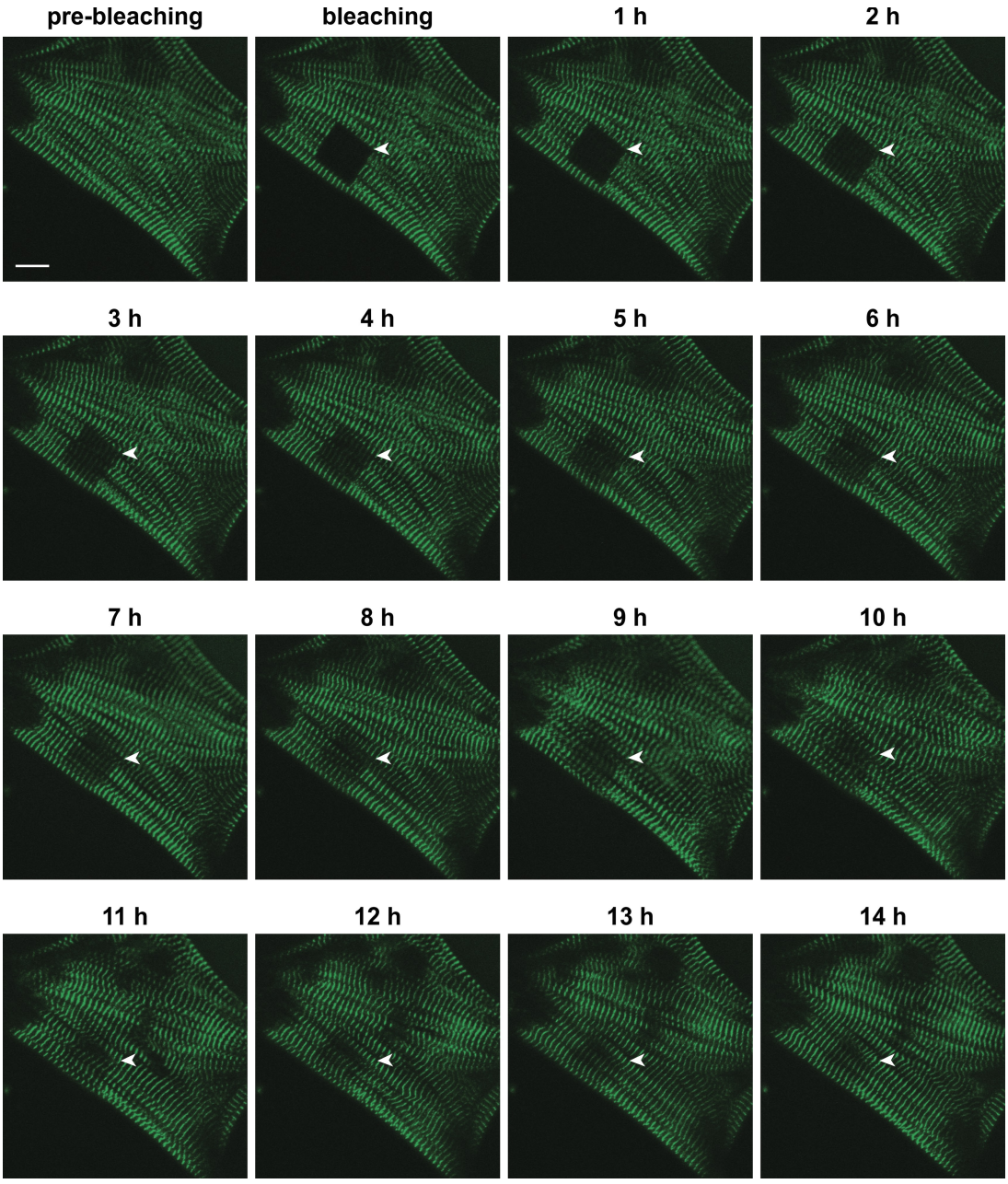

Figure S2. **Time-lapse images documenting the fluorescence recovery of titin-eGFP.** FRAP analysis was performed to follow titin's mobility over time. Images were taken before bleaching, immediately after bleaching, and hourly until 14 h after photobleaching when recovery had reached a steady state. Bleached titin-eGFP molecules were replaced by fluorescent titin-eGFP and the recovery appeared homogeneous throughout the investigated area with slightly faster recovery at the edges where neighboring fluorophores are more abundant than in the central area. There were no obvious structural changes or rearrangements of the myofibers in the period reported. Bar, 10 µm.

Published May 9, 2011

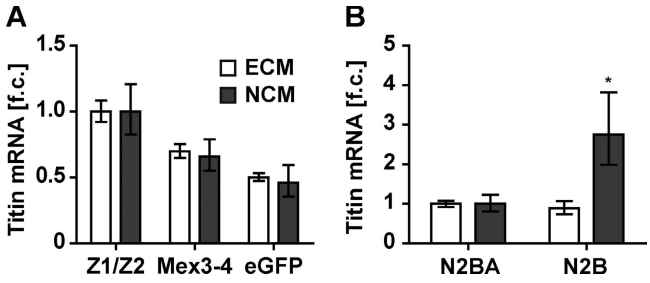

Figure S3. **Titin isoform expression in embryonic and neonatal cardiomyocytes.** Embryonic and neonatal cardiomyocytes (E13.5 and P2, respectively) were isolated, cultured for 3 d, and used for the analysis of titin isoform expression by qRT-PCR. (A) Expression of the Z-disc region (Z1/Z2), the M-band region (Mex3-4), and the 3-prime eGFP was not significantly changed between embryonic and neonatal cardiomyocytes. (B) After birth the large N2BA titin isoform was replaced by the smaller N2B isoform. N2B expression was significantly increased in neonatal as compared with embryonic cardiomyocytes ($n = 3$). *, $P < 0.05$. Error bars indicate SEM.

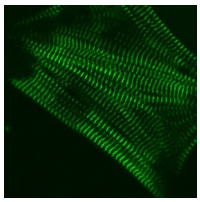

Video 1. **Time-lapse video: fluorescence recovery of titin-eGFP.** FRAP analysis was performed to follow titin's mobility over time. Bleached titin-eGFP molecules were replaced by fluorescent titin-eGFP and the recovery appeared homogeneous throughout the investigated area with slightly faster recovery at the edges where neighboring fluorophores are more abundant than in the central area. Photobleaching experiments were performed with a laser-scanning confocal microscope (LSM 510 Meta; Carl Zeiss). Frames were taken every hour for 14 h.